Experimental and computational study of the aerodynamic sound generation in the lung airway represented by simplified and realistic model

GABRIEL PRAMUDITA SAPUTRA

SEPTEMBER 2016

Experimental and computational study of the aerodynamic sound generation in the lung airway represented by simplified and realistic model

A dissertation submitted to

THE GRADUATE SCHOOL OF ENGINEERING SCIENCE

OSAKA UNIVERSITY

in partial fulfillment of the requirements for the degree of

DOCTOR OF PHILOSOPHY IN ENGINEERING

By

GABRIEL PRAMUDITA SAPUTRA

SEPTEMBER 2016

ABSTRACT

One of the efforts to improve the accuracy and objectivity of the respiratory diseases detection by lung sound analysis is by improving our knowledge regarding the sound generation mechanisms. Here, aerodynamic sound generation studies were performed to reveal the factors affecting the sound generation in tracheobronchial models. In the beginning, a simplified T-branch model was utilized as a simplification of the airway bifurcating branching geometry. A constriction was located on the mother branch to recreate a bronchoconstriction of the airways. The acoustic sound pressure and the flow fluctuation at a point downstream the constriction were measured while varying the constriction severity and the airflow rates. As results, a clear relationship between the Reynolds number and the overall sound pressure level was observed. A minimum Reynolds number of 4000 was required to generate 2 dB sound. The increase of the turbulence strength was also found as the Reynolds number increase. However, the relationship between the Reynolds number and the turbulence strength was not as clear as the overall sound pressure level. This may indicates that a single point measurement of the flow fluctuation may be not enough to describe the relationship between the flow fluctuation and the generated sound. To regenerate the flow condition in a more realistic geometry, a silicone airway model based on CT-image based image of an 11 years old boy was constructed. The model is a silicone in a rectangular prism shape with tracheobronchial cavity. Acoustic pressure of 680 points was measured and mapped when air flowing through the airway cavity at inspiratory and expiratory direction. This enables us to locate the original aerodynamic sound sources as fluid moving through the tracheobronchial without considering the complexity of the tissues and bones in the chest anatomy. It was found that the characteristics of the sound is different between inspiration and expiration. In expiration, a wide band sound frequency ranging from 1000 Hz to 4000 Hz can be detected, while in the

inspiration, the sound spectra were found in the range of 1000-2000 Hz. However, a similar location distribution of the sound sources was observed. At frequency less than 1500 Hz, the trachea region shows higher sound level compared to the small airways, however, at frequency higher than 2000 Hz small airways are generating higher sound level compared to trachea and main bronchus region. This may indicate that the generated sound depends on the geometry and the dimension of the airways. To observe the flow condition relying on the sound generation in the silicone airway model, computational fluid simulations were performed for the same geometry with the same rate used in the measurement. Calculating the sound source terms based on Lighthill acoustic analogy, the locations of sound sources and the frequency dependency of the sound sources were observed. Similar results of the sound source distributions between simulations and experimental measurements were obtained. The sound in trachea region has lower frequency characteristics compared to the sound observed in the small airways. The computational simulations show a different flow condition related to the sound generation in expiration and inspiration. In the expiration case, flow collision, flow impingement, and flow separation are related to the location of the sound sources. While flow impingement and flow separation are the main mechanisms contributing in the sound generation in the inspiration maneuver.

TABLE OF CONTENTS

INDEX TO FIGURES

Chapter 1

Introduction

1.1. A REVIEW TO THE STUDY OF LUNG SOUND ANALYSIS

Human respiratory system has the main function of the exchange between oxygen from the air with the carbon-dioxide from the blood. Figure 1-1 shows the anatomy of the human respiratory system starting from the nasal and mouth cavity to the bronchioles which distributes the air to the alveoli. The respiratory system can be classified into upper respiratory tract and lower respiratory tract. The upper respiratory tract consists of nose, mouth, pharynx, and larynx. The lower respiratory tract is started from the larynx down to the alveoli. The lower respiratory system can be categorized furthermore into conducting airways, whose main function is to distribute the air throughout the lung, and respiratory zones, where the oxygen-carbon dioxide transfer occurs. Respiratory diseases were known to change the structural and geometrical properties of the respiratory airways [2]–[5] and affecting the breathing efficiency. A classic method to diagnose these respiratory diseases is performed from by listening to the chest sound [6], [7].

The topics of the lung sound observation and the generation mechanisms were in a great concern especially after Laennec proposed the application of stethoscope for the auscultation of lung sound [6]. Laennec also introduce some terms of the sound measured on the chest surface such as tracheal sound, bronchial sound, and vesicular sound for the normal lung, and stridor, wheeze, and crackles for the abnormal lung. Researchers following this study realized that the respiratory diseases change the sound generation and the propagation characteristics from the sources to the chest surface. The understanding of the phenomena behind the sound

generation and its propagation behavior through the chest are therefore required to improve the accuracy and the objectivity of the sound observation activity.

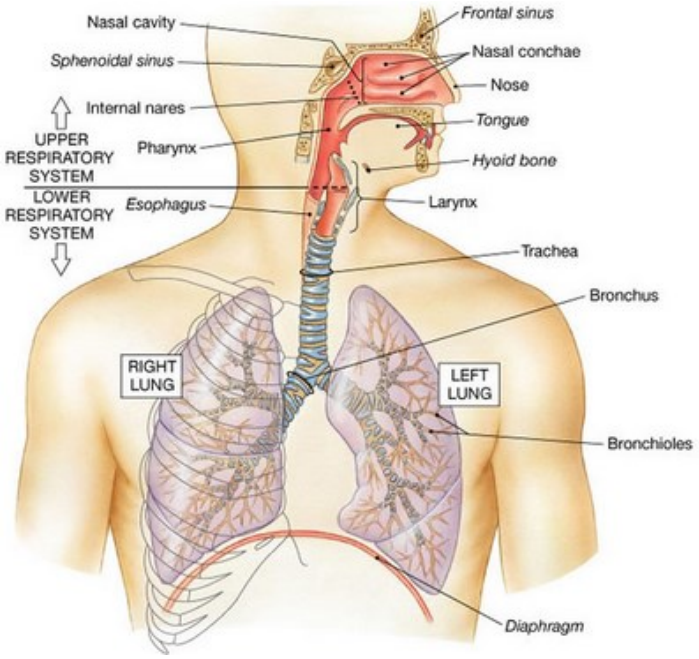

Figure 1-1. The anatomy of human respiratory system [8].

In general, sound can be produced as the results of the vibration of a surface or the fluctuation of a fluid flow which propagates through the surrounding material. The sound generated as the byproduct of the airflow fluctuation or the turbulent fluid motion is also known as the aerodynamic sound [9], [10]. Main component in the production of the aerodynamic sound is the fluctuation as result of instability. This kind of aerodynamic sounds can be found in the musical instruments such as flute and recorder which sound is characterized by the air flowing through a cavity, or a sharp edge.

These two kind sound generation mechanisms (i.e. aerodynamic sound generation and solid vibration sound) can also be found in generation of the lung sound considering the complexity of the flow pattern and the combination of the soft and hard material of the lung airways. Some of existing studies indicate that the main contributing factor of the sound

generation in a normal respiratory airway is the air flowing in the airway [6], [11]–[15], while some other mechanisms (i.e. the interaction between the flow and the solid structure) give the contributions to the generated sound in the abnormal condition such as crackles [16]–[19], stridor [6], [12], [14], or wheezes [20]–[23].

In the previous time, the study of aerodynamic sound generation in the lung airway was not very common and researchers were more interested to the gas flow pattern and distribution. The gas flow pattern in the airway has been performed experimentally and theoretically such as described in [24], [25], numerically [26]–[28], and reviewed concisely in [1], [29]. These studies are focusing mainly on the flow pattern and their contribution to the particle dispositions characteristics [27], [30]–[36]. Nevertheless, some studies of the lung sound generation can be found in [20], [37]–[41]. In 1960s, a detailed investigation of sound waveforms contained in a lung sound was performed by P. Forgacs [14], [15] denoting the first systematic measurements of respiratory sounds [42]. The sound generated in the lower generation and smaller diameter airway are not completely understood, however, it is generally accepted that the turbulent flow in the trachea and other large diameter airway as one of the sound source while no clear evidence can answer the question of how and where the sound was generated. Murphy [7] reviewed some possible origin of vesicular and bronchial sounds based on previous studies [11], [14], [15], [43], [44]. Only Hardin [43] completed the sound study with a theoretical observation of the vortex sound, although the proof that the vortices themselves produce the sound or the spectral component of the lung sounds comes from the geometry of the airway and velocity of the flow is still not convincing.

An effort to explain the sound generation mechanisms in the airway is also studied by Austrheim [45]. By changing the component of the flowing fluid, they observed that the inspiratory vesicular sound production mechanism is independent with the gas density, while the tracheal and expiratory sound appear to be produced by a density dependent mechanism,

such as turbulent sound. However, Mahagnah & Gavriely found that the lung sound transmission was not affected by the gas density in a normal men [46].

In the case of the abnormal sounds, more effort was given in the wheeze and crackles generation mechanisms was found since it was commonly found and easy to identify. Wheeze sound that commonly occurs in the asthma case or forced expiratory movement was discussed deeply by Meslier [47]. The hypothesis of the origin of the sound including the eddy-induced wall oscillations with or without airflow limitation was presented. The fluid dynamic fluttering theory and the clinical condition related to wheezes were also discussed thoroughly. Forgacs [14] initially suggested that wheezes can be analogous to the orchestral wind instruments or like the mouth organ or toy trumpet where the frequency depends entirely on the mechanical properties of a reed consisting of two solid structures in apposition. In the following years, Grotberg [39] and Gavriely [22] proposed that wheezes are produced by fluttering of the walls and fluid together as the airflow pass through a collapsible tube. On the other hand, the crackles sound are considered to be the sound of the sudden airway closure during expiration and sudden airway reopening during inspiration [17].

The properties of the abnormal lung sound are clear and easy to be distinguished from the properties of the normal sound [13], [48]–[50]. However, in the transition between the normal and the abnormal lung condition, it is believed that the sound properties were also changed, but the main generation mechanisms were still sound generated aerodynamically. Therefore, understanding the sound generated aerodynamically and its alteration from the normal lung to the diseased lung may be useful to aid the early detection of the respiratory diseases. In this study, the sound generated aerodynamically is discussed comprehensively to provide clarity of the sound generation mechanisms of the lung sounds.

1.2. BRIEF INTRODUCTION TO AERODYNAMIC SOUND ANALYSIS

In the theory of the aerodynamic sound, the airflow fluctuation or the turbulent fluid motion is considered to be the source of the sound sources. A regular eddy pattern is responsible for the sound production in a musical instrument at low Reynolds number [51]. At high Reynolds number, an irregular turbulent motion is responsible for the generation of the wind and of the jet sound of airplanes [9], [52]–[54] or in the generation of Aeolian tones sound of Shinkansen pantograph [55]. Remembering some factors contributing to the aerodynamics sound generation, i.e. Reynolds number, Mach number, and the size of the eddies of the flow, we consider the possibility of the application of this analysis in the aerodynamic sound generation by the flow in the airway.

In 1954, Lighthill published a method to analyze the sound generated aerodynamically known as the Lighthill's acoustic analogy where the non-stationary fluctuations of the stream are represented by a distribution of quadrupole source in the same volume whose strength per unit volume at instant is

$$\boldsymbol{\tau} = \rho\, \overline{\mathbf{u}'\mathbf{u}'} + (p - c_0^2\rho)\delta_{ij} \qquad \text{(eq. 1-1)}$$

placed in a medium at rest. Here $\boldsymbol{\tau}$ is the Lighthil stress tensor, ρ is the density, $\overline{\mathbf{u}'}$ is the fluctuating component of the fluid velocity, p is the pressure, and c_0 is the speed of sound. This definition leads to some important definitions of the sound sources related with the sound generated aerodynamically. A turbulence without a mean flow has an acoustic power output, nevertheless, turbulence of a given intensity can generate more sound in the presence of a large mean shear. In addition, the size of the effective quadrupole may become comparable with the acoustic wave-length at subsonic Mach numbers. One of the important conclusion of the Lighthill's theory is that the aerodynamics sounds can be predicted by the Reynolds number, Mach number, and the size of the quadrupoles generated by the turbulence.

1.3. MOTIVATION AND AIM OF THIS THESIS

The flow condition inside the tracheobronchial airways might be very complex caused by the complexity of the airway geometry. Edge sound, cavity sound, trailing edge sound, jet flow, and vortex sound are to name a few of the cases commonly studied in the aerodynamic sound field which is possible to be found in the lung airway case [56]–[62]. Sharp edge at the carina, wavy profile of the trachea, and constriction by the airway inflammation may contribute to the sound generation in a similar mechanisms.

In this study, the flow condition in the airway is investigated in the relationship to the aerodynamic sound generation. By reproducing similar flow structure using simplified and realistic model, this thesis aims to provide a comprehensive analysis of the sound generation mechanisms. The understanding of the sound generation mechanisms may help the prediction of the acoustic alteration of the lung sound by improving the knowledge of the factors affecting the sound characteristics.

A simplified model represented by a T-branch circular channel was constructed in order to explain the effect of a constriction in the channel that may create a jet-flow structure [28], [63], [64] with a flow impingement that can be found in a branching point. This model was considered to be able to represent the flow condition of a jet flow in a single branching point which is the fundamental geometry in a lung airway system.

A CT-image based tracheobronchial geometry was studied experimentally and computationally to understand the more realistic flow condition in the tracheobronchial system which is absolutely more complex than the T-branch configuration. An acoustic visualization technique based on the sound pressure field measured by a microphone array system was introduced in order to visualize the sound pressure distribution and the location of the sound source of the airway model. This method was performed by realizing that the sound pressure level will reach its maximum value at the nearest location to the source. Computational fluid

dynamic simulations were performed to explain the flow condition related with the sound generation in the lung airway by observing the velocity fluctuation.

1.4. OUTLINE OF THE THESIS

This thesis is composed of five chapters. In the first chapter, the introduction and a brief review of the respiratory flow, the lung sound analysis and aerodynamic sound study are introduced. In Chapter 2, a simplified model of the airway represented in a T-branch geometry is presented. Chapter 3 describes the localization of the sound sources in a realistic silicone tracheobronchial model by using a microphone array system. In Chapter 4, a computational fluid simulation of the flow inside the tracheobronchial model is presented. The general summary and research contribution of current study are concluded in Chapter 5.

Chapter 2

Acoustic and fluid flow measurement of T-branch model

2.1. INTRODUCTION

The study of aerodynamic sound generation in the human tracheobronchial system is started with the simplified model in this thesis. A simplified model provides the fundamental flow characteristics required to generate sound in the branching configuration. The utilization of a simplified model in understanding the flow characteristics of the human airway has been performed since a long time ago. In 1963, Weibel introduced a symmetric bifurcation model of the human airways [65]. This symmetric model has been used to describe the flow pattern and to understand the mass flow distribution in the bronchial system [1], [66]. In the recent time, using a symmetric double bifurcation [33] or three-generation bifurcating geometry [67], researchers studied the flow characteristics in order to predict the mass flow ratio between each branch and also the aerosol disposition pattern in response to the inlet boundary condition and different condition of the constriction. This symmetric model has been considered to be not capable to represent the realistic branching pattern in the human bronchial airway. Based on the technique applied in describing the rivers branching and the preliminary study of the morphology of human bronchial tree [68], [69], Horsfield proposed an asymmetric bronchial model in 1971 [70]. This model is considered to be proper to represents the geometrical characteristics of the human bronchial airway, however, the asymmetric branching configuration leads to the complexity of the flow analysis. For the sake of the simplification, many groups still use the symmetric model to analyze the flow pattern in the bronchial airway.

The fundamental factors related to the sound generation in the tracheobronchial system are studied in this chapter. A simplified T-branch model was chosen to represent the branching of the airway. This model was considered to be enough in the aeroacoustics study since the basic phenomena of the flow dynamics in an airway branch can be found instead of the simplicity in the fabrication and design. Several factors which are related to the sound generation level are studied: the constriction of the airway and the air flow rate. The constriction at the mother branch is located to represent the bronchoconstriction. Several flow rates are applied to represents different flow speed in the breathing maneuver. Varying the flow rates and the constriction severities, and measuring the flow fluctuation downstream the constriction region, the flow condition required to generate the sound in the T-branch model was analyzed and discussed in this chapter.

2.2. METHOD

A T-branch configuration shown in Figure 2-1 was constructed by casting technique using a 3D printed mold (Zprinter 250; 3Dsystems, South Carolina, USA). Four different constricted tube models were constructed: no constriction model, 25% constriction, 50% constriction, and 75% constriction. This constriction percentage was calculated based on the diameter ratio of the constricted region (D') to the normal tube (D_0) based on the definition shown in Figure 2-2. The constricted tube was placed at the mother branch while no constriction tubes are placed in two daughter branches. Main diameter (D_0) of the T-branch model is 7 mm while the length of each branch is 30 mm. Other dimensions used for the construction of the T-branch model are shown in Figure 2-2.

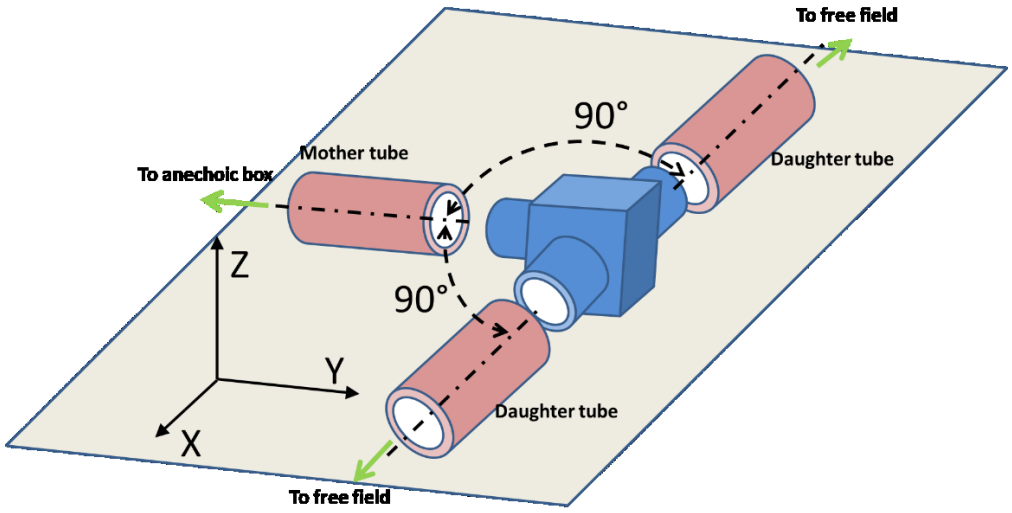

Figure 2-1. The T-branch model configuration.

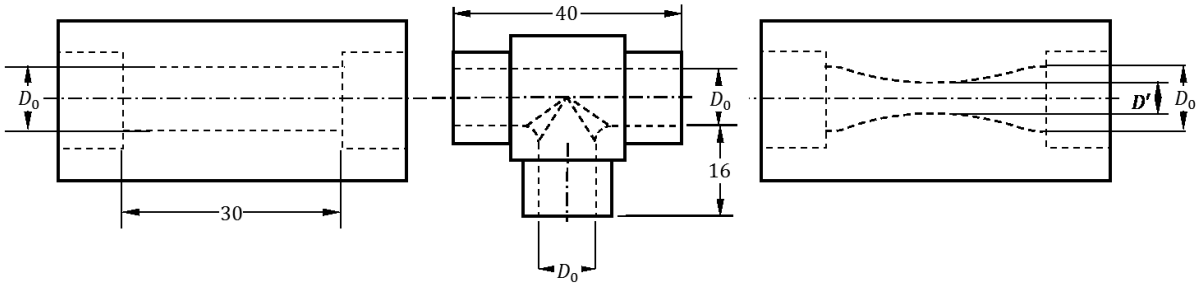

Figure 2-2. The dimensions used for the construction of the T-branch model.

An air supply system (Figure 2-3) consisted of an air compressor (Kapsel-con YC-4RS; Hohmi, Japan), an air tank (Anest Iwata SAT-120C-140l Anest Iwata Corp., Japan), and an air flow meter (Azbil CMS0050; Azbil Corp., Japan) was used to supply the air with flow rate of 5, 10, 15, 20, 25, and 30 L min^{-1}. These values are the common flow rate values used in many literature for a normal and diseased lung study [36], [71]–[77]. An anechoic expansion box made of wood with anechoic material and honeycomb structure inside the box are used at the end of the air supply system just before the T-branch model to reduce the fluctuation and the noise generated by the air flow meter and the valve.

In order to observe the relationship between the flow condition and the level of the generated sound, sound pressure measurements and flow fluctuation measurements were performed. The sound pressure was measured by using a microphone, while the flow fluctuation was measured by using a hot-wire anemometer. A free field microphone (Bruel Kjaer 4939, attached to Bruel Kjaer 2670 pre-amplifier; Brüel Kjær Sound and Vibration Measurement A/S, Denmark) was located at 8 cm above the test model. The measurements were sampled at rate of 20000 Hz and 16 bit depth. The measurements were performed inside an anechoic cover size of 90×90×92 cm^3. The measured sound was processed in MATLAB R2012a (MathWorks, Inc., USA) using 2048 point FFT function, 0.5 overlap coefficient, and Hanning window. Ensemble averaging was performed using 50 data sets for each measurement. To characterize the measured sound, the Overall Sound Pressure Level (OASPL) was calculated following

$$\mathrm{OASPL} = 20\log_{10}\left(\frac{\sqrt{\sum_{i=a}^{b}\left(P_{ref}\times 10^{PSD(f_i)/20}\right)^2}}{P_{ref}}\right), \qquad \text{(eq. 2-1)}$$

where P_{ref} is the reference pressure equal to 2×10^{-5} Pa, $PSD(f_i)$ is the Power Spectral Density (PSD) value in decibels of the corresponding frequency f_i obtained from the FFT calculations, and *a* and *b* are the lower and upper limits of the frequency of interest, respectively.

Flow fluctuation generated by the constriction was measured by a hot-wire anemometer (Kanomax 0251R-T5; Kanomax Inc., Osaka, Japan). The location of the anemometer was shown in Figure 2-4. The flow fluctuation itself was characterized by the turbulence strength calculated using

$$TS = \sqrt{\frac{1}{n}\sum_{i-1}^{n}(u'_i)^2} \qquad \text{(eq. 2-2)}$$

where n is the number of sample, and u' is the fluctuating component of the velocity.

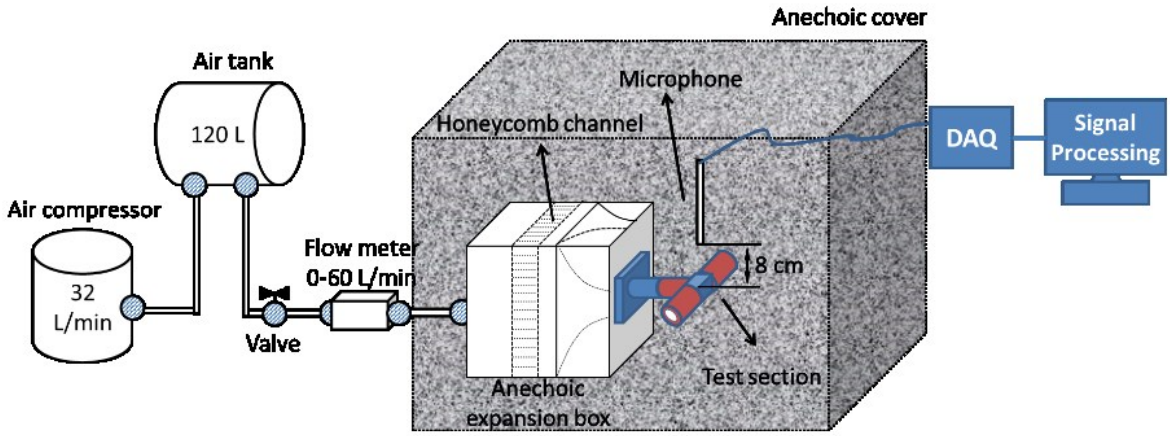

Figure 2-3. Experimental setup used for sound measurement.

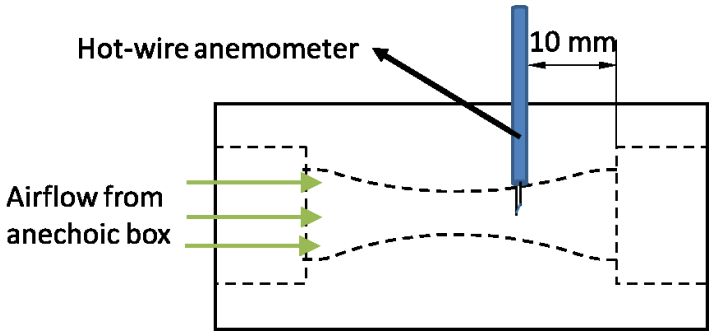

Figure 2-4. Location of the hot-wire anemometer measurements at the mother branch.

The relationship between the local Reynolds number Re with the OASPL and the turbulence strength (TS) was also discussed. This local Reynolds number was used to describe the flow condition in the constriction region. The local Reynolds number calculated at the constriction was calculated following the equation

$$Re = \frac{\rho U D_h}{\mu} \qquad \text{(eq. 2-3)}$$

where ρ indicates the density of the fluid, U the average velocity magnitude, D_h the hydraulic diameter of the channel which is the minimum diameter in the constriction region, and μ is the dynamic viscosity of the air.

2.3. RESULTS

The Power Spectral Density (PSD) of the sound measured at 5, 15, and 25 L.min^{-1} for each constriction model is shown in Figure 2-5. In each model, a minimum required flow rate to generate a detectable sound can be observed. At no constriction, the minimum flow rate is 25 L.min^{-1}, in 25% and 50% constriction model a flow rate of 15 L.min^{-1} is required to observe the first increase of the PSD. However, in the 75% constriction model, at flow rate of 5 L.min^{-1} can generate an increase of the PSD up to 10 dB in frequency greater than 1300 Hz. It is also important to note that the frequency distribution in a model was tend to be constant instead of the flow rate value.

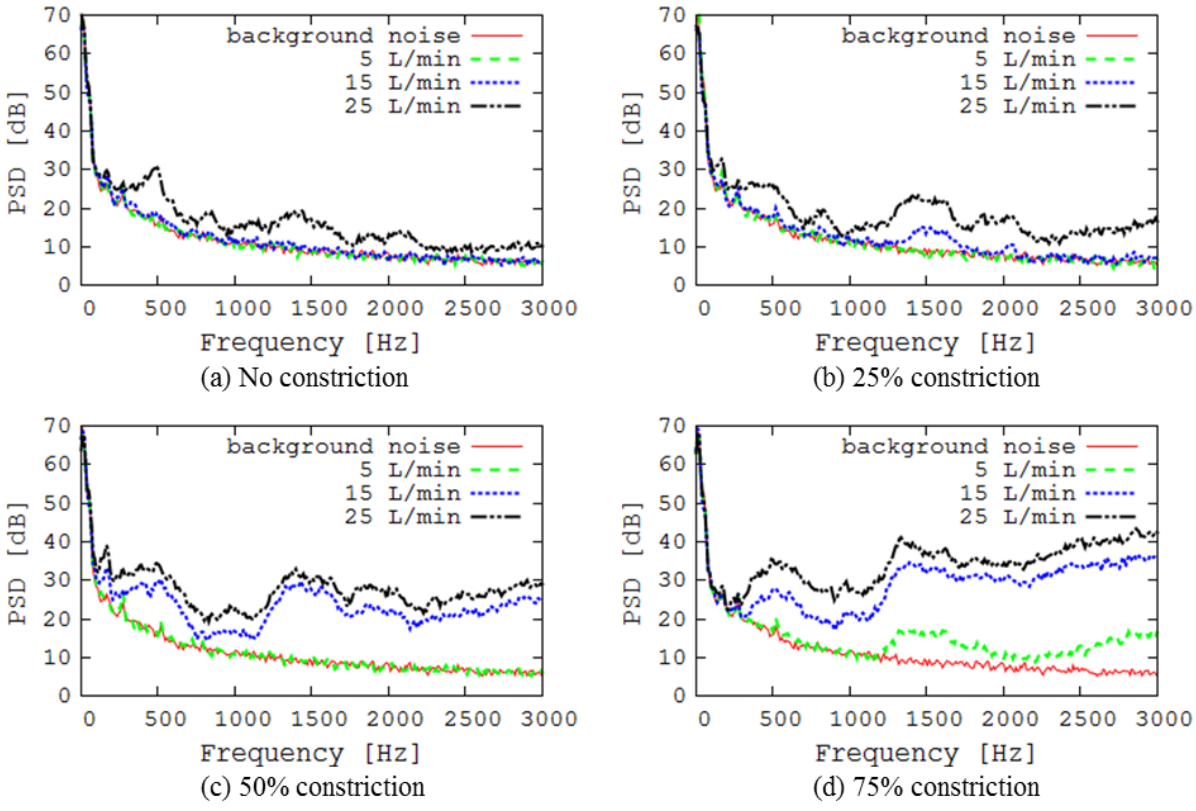

Figure 2-5. The PSD distribution of sounds for all models in four flow conditions: (a) no constriction model, (b) 25% constriction model, (c) 50% constriction model, (d) 75% constriction model at different flow conditions shown in different line styles. Background noise indicate the sound measured at no flow.

The measured turbulence strengths (TS) at 10 mm downstream the minimum constriction are shown in Figure 2-6. The increase of flow rates was followed by an increase of the TS in all models. In the no constriction model and 25% constriction model, a maximum TS value of 0.1 $m.s^{-1}$ can be observed at flow rate more than 20 $L.min^{-1}$ in no constriction model and 15 $L.min^{-1}$ in 25% constriction model. In 50% constriction case, TS value more than 0.2 $m.s^{-1}$ was found at flow rate more than 25 $L.min^{-1}$. At constriction level of 75%, a TS value of more than 1 m.s-1 was observed at flow rate more than 10 $L.min^{-1}$.

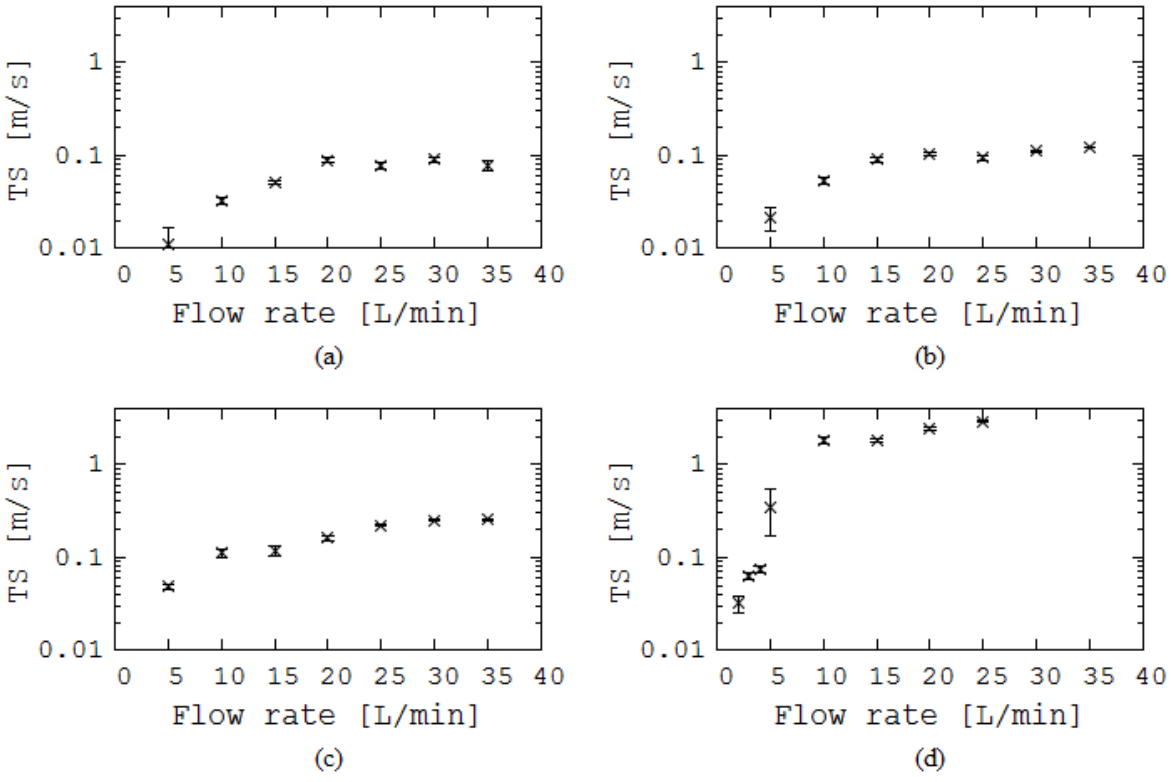

Figure 2-6. Turbulence strength at several flow rates measured in (a) no constriction model, (b) 25% constriction model, (c) 50% constriction model, and (d) 75% constriction model.

The relation of the OASPLs of the sound generated by the T-branch model at six frequency ranges (1-200 Hz, 200-400 Hz, 400-600 Hz, 600-800 Hz, 800-1000 Hz, and 150-10000 Hz) with respect to the Reynolds number calculated at the constriction are shown in Figure 2-7. From these figures we observe that the OASPL of each model did not increase in the frequency range of 1–200 Hz, even though the Reynolds number had reached its maximum value observed in this study. In the frequency ranges of 200–400 Hz, 400–600 Hz, 600–800 Hz, and 800–1000 Hz, we can observe a continuous increase of the OASPL as the Reynolds number increase. A Reynolds number of more than 4000 was generally required in all ranges in order to generate a 2 dB increase of the OASPL. In the range of 150-10000 Hz (Figure 2-7(f)), at Reynolds number higher than this, the OASPL are increasing continuously with a saturation behavior at Reynolds number more than 14000. Turbulence strength of the flow fluctuation at 5 mm downstream the constriction are shown in Figure 4. An increase of TS can be found as the Reynolds number increase in all cases. A TS less than 0.2 $m.s^{-1}$ can be observed in the no constriction, 25% constriction, and 50% constriction case. In the 75% constriction case, an increase of the TS can be observed as the Reynolds number increase with TS reaching 2 $m.s^{-1}$ for the maximum Reynolds number observed in this study.

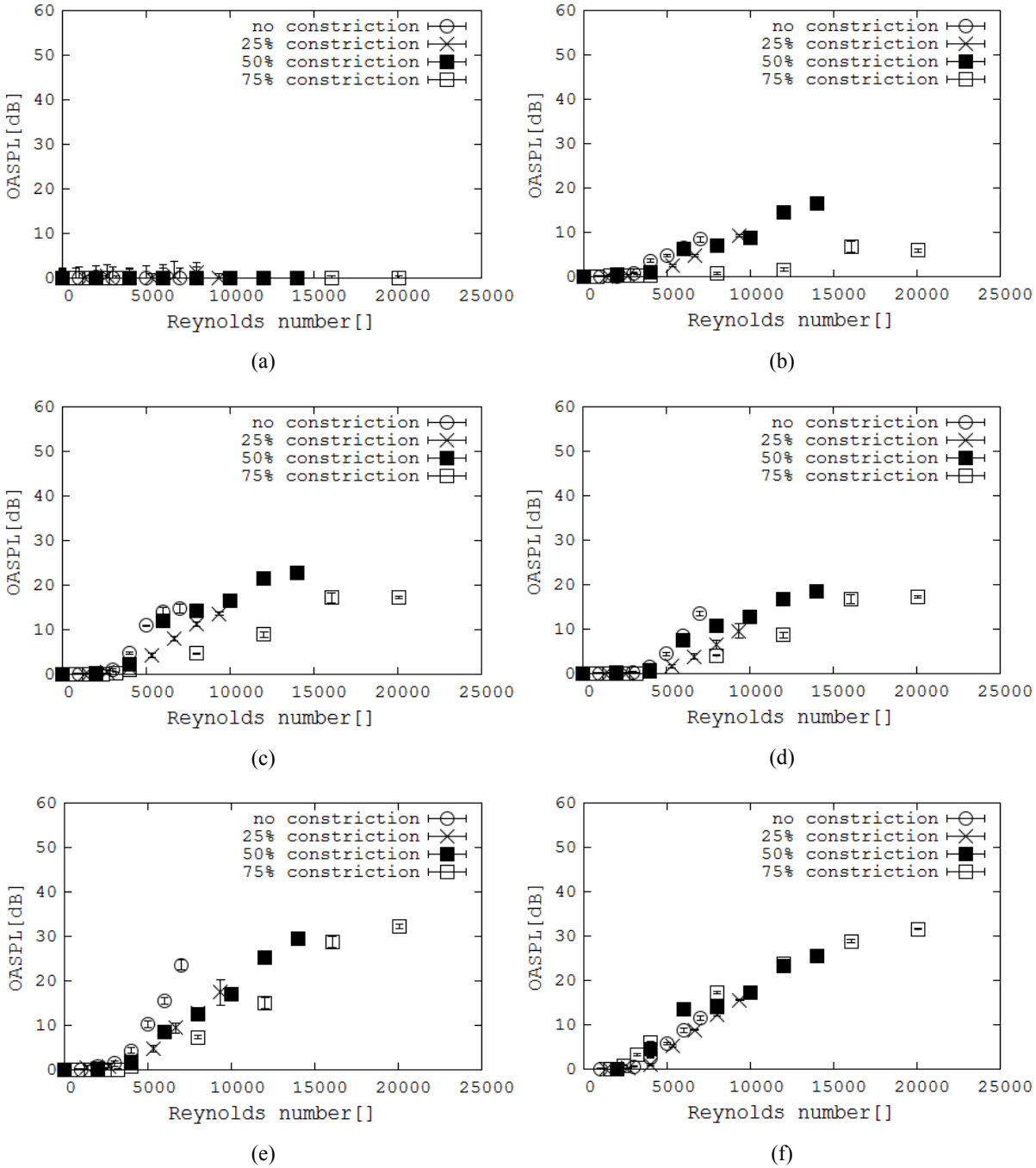

Figure 2-7. OASPL of the sound measured from the T-branch model. (a) 1–200 Hz, (b) 200–400 Hz, (c) 400–600 Hz, (d) 600–800 Hz, (e) 800–1000 Hz, (f) 150–10000 Hz.

2.4. DISCUSSION

The increase at low frequencies in low-constriction models can be related to the flow velocity and the geometry of the models. A low-constriction level means that the diameter is still relatively wide at the constricted region. This large diameter corresponds to a lower-frequency region. A large diameter leads to a low-flow velocity and low-vorticity speed, which may generate lower-frequency sound. A higher constriction level leads to an increase in the flow velocity and therefore more energy are contained in the flow, which in turn generate the flow instability which is one of the sources of the sound. The combination of high flow velocity and the constriction geometry results in an increase of the sound at 200–800 Hz frequency range. In higher constriction level model, compressibility of the flow must also be considered and this may lead to a significant increase in higher frequency range. Physically, high frequency sound might be reduced during lung sound measurement from the chest surface because lung parenchyma acts as a low-pass filter, with a general threshold frequency of 1000 Hz [78], or 2000 Hz [71].

Combining the TS measurements (shown in Figure 2-6) into a single plot, we obtained a relationship between TS and Reynolds number, as presented in Figure 2-8. From the TS measurements, we found that when measured in the center of the tube, 5 mm downstream from the minimum constriction diameter, the flow showed a small fluctuation in the cases of no constriction, 25% constriction, and 50% constriction. This means that in the vicinity of the measurement location, the flow is relatively stable (i.e., not fluctuating or with only small turbulence) in the case of less than 50% constriction, even though the Reynolds number was as high as 14000. In the case of 75% constriction, the flow becomes unstable and the fluctuation level is proportional to the Reynolds number of the flow. However, if we look closely at the no constriction case at 15 $L.min^{-1}$, a discrepancy appears and a sudden increase of the TS can be found, which also appears at 75% constriction under a 4 $L.min^{-1}$ flow rate. This discrepancy

may be due to interference from the measurement instrument, which may affect the flow inside the silicone tube and result in high flow fluctuation around the hot wire anemometer.

Flow fluctuation is one of the known mechanisms of lung sound generation, as proposed by Lighthill [9]. Additionally, constriction has been demonstrated to be a source of flow fluctuation [79]. The fluctuation of the velocity component **v** in the Lighthill stress tensor ($\mathbf{T} = \rho_0 \mathbf{vv}$) appears as one of the sources for the pressure disturbance that propagates through the fluid in the Lighthill equation (eq. 1-1). The velocity fluctuation, indicated by the turbulence strength term, may therefore indicate the aeroacoustic sound source. The geometry of the constriction was responsible for generating a high-flow velocity and high-velocity fluctuations, which were seen when the channel diameter was reduced. This mechanism may explain increased sound in patients with bronchoconstriction. Comparing the flow fluctuation analysis and the OASPL analysis shown in Figure 2-7 and Figure 2-8, we saw that the OASPL did not follow similar behavior to the TS; however, the OASPL has a defined relationship to the Reynolds number of the flow. The increase of the OASPL in the no constriction, 25% constriction, and 50% constriction model was not followed by an increase of the flow fluctuation. In our system, the flow fluctuation appeared in some regions inside the models, but its exact location has not yet been detected. The measurements taken from a location downstream from the constriction did not agree with the OASPL data.

In a real human lung, bronchoconstriction is known to change the properties of the lung sound ([49], [78], [80]), although specific parameters that can objectively predict the bronchoconstriction level are still under investigation. Bronchoconstriction can appear at several locations in peripheral airways simultaneously. This situation leads to an increased number of sound sources, and therefore smaller Reynolds numbers are required for the sound detection, but more complex frequency distributions are generated. From our observations, we suggest that this increase in sound sources will affect the medium frequency component of

200–800 Hz for constrictions of less than 50%. In normal condition, assuming a high respiratory flow rate (100 $L.min^{-1}$), Reynolds numbers of greater than 4000 might appear only up to the third generation of the airway [25]. In a diseased lung, these Reynolds numbers might appear in higher generations because of the appearance of constriction in the lung airway, leading to a spread of turbulence sound source locations.

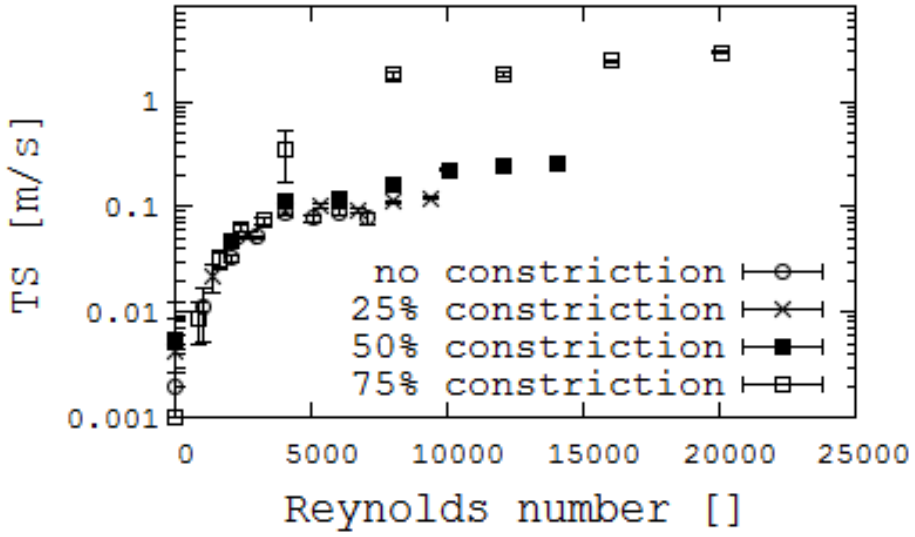

Figure 2-8. Turbulent strength measured 5 mm downstream the constriction.

2.5. SUMMARY

We performed an experimental study to understand the factors affecting sound generation and alteration in a bronchoconstriction. Using T-branch models as a representation of airway branches, and a constricted tube as a representation of airway bronchoconstriction, we observed changes in sound PSD caused by changes in flow rates and changes in frequency distribution produced by the constriction level. The combination of the flow rates and the constriction changes the Reynolds number of the flow, and the constriction level itself determines the sound

characteristics. Constriction levels of less than 50% tended to increase the OASPL within a frequency range of 200–800 Hz, while constriction levels of 75% tended to increase OASPL at frequencies greater than 800 Hz. A minimum Reynolds number of 4000 was needed to generate sound with OASPL of 2 dB in our experiments. At Reynolds numbers lower than this, the OASPL was relatively small, and at higher Reynolds numbers the OASPL increased drastically. The constriction is known to increase both the Reynolds number of the flow and the OASPL results; however, flow fluctuation measurements at the center of the tube, 5 mm downstream of the constriction, did not show the same trends. Lighthill's theory predicts this location to be a sound source, but our results suggest that the flow fluctuation might appear not only at the assigned measurement point, but also somewhere else further downstream from the constriction. Additionally, we observed that a constriction in the lung airway may increase the frequency distribution of the generated sound. A clear indicator of the constriction is the increase of the OASPL generated by the high Reynolds number flow, which is generated by a high flow rate breathing maneuver. This increase of OASPL, if measured from the human chest, could therefore be useful in detecting the existence and severity of a constriction. In the future, studies using more physiologically accurate models could ascertain the validity of our current analysis for in-vivo situations.

Chapter 3

Acoustic visualization of the silicone lung airway model

3.1. INTRODUCTION

The T-branch model used in Chapter 2 showed us the requirement of some flow condition characterized by the non-dimensional Reynolds number to generate sound. A Reynolds number of 4000 was required to generate a 2 dB sound level for the frequency range of 150-10000 Hz. The flow in a similar Reynolds number was used in a more complex model which is based on a CT-image data to reproduce a more realistic flow condition. In this chapter, we tried to apply a mapping of acoustic pressure to locate the aerodynamic sound sources generated by the flow in a silicone tracheobronchial model using a microphone array system.

An acoustic mapping method was commonly used in order to localize the source of the noise by using microphone array and beamforming or holography technique. However, the microphone array size may limit the frequency and spatial resolution [81]–[84] of the acoustic map. To overcome this limitation, researchers tried to apply the sensor array technique (microphone or accelerometer) in the lung sound study by simply calculating the total vibration energy measured by each sensor [5], [85]–[88]. This method was known to be able to detect wheezes, crackles, and stridor depends on the algorithm used for processing the data. However, no explanation of the sound generation mechanisms was given by this method since researchers only focus on the acoustic signal processing and device sensitivity improvement.

In this chapter, a localization method of the sound generated aerodynamically in a silicone airway model is presented by utilizing a microphone array system. The location of the sound

source and the characteristics of the generated sound are measured by detecting the sound pressure profile generated from a silicone airway model. The sound generated by the air flowing in the respiratory system is commonly used in the diagnosis process of the lung condition. Understanding the location of the sound generation and the response to a varying condition of the airway may help physician in determining the real condition of the respiratory system. The normal airway condition is assumed in this chapter in order to observe the base line of the sound generated by air flowing in a tracheobronchial configuration.

3.2. METHOD

A realistic silicone lung-airway model was constructed based on CT-scan images of an 11-year old boy with light asthma. A written informed consent was obtained from the studied subject or their legal guardians, which protocol has been approved by the ethics committee of Minami Wakayama Medical Center. The CT-images were taken in the time that the asthma was inactive and maximum inhalation state using Toshiba Aquilion (Toshiba Medical System Corporation). The image data consist of 590 image slices steps of 0.5 mm and in plane resolution of 512×512 pixels (spatial plane resolution 0.586 mm×0.586 mm. Multi-directional segmentation [89] applied to the CT images yields to the segmented voxel data of the lung airway from trachea up to tenth generation of airway branch according to the Horsfield rule [70]. A total number of 39 brohchi ends were constructed with minimum diameter of around 1 mm. The segmented voxel data were smoothed in AMIRA 5.4.2 (Konrad-Zuse-Zentrum, Berlin, Germany, and Visage Imaging, Victoria, Australia), and smoothed airway surface data were constructed as the basic geometry. Some modification was applied in order to accommodate the inlet and outlet location for the silicone airway model. The modified

geometry was used to construct the airway model for experimental measurement and the computational simulation.

Based on the airway surface data, a bulk silicone airway model size of 115×185×60 mm^3 was constructed (Renaissance of Technology Corp., Japan) with a trachea, and 39 bronchi shown in Figure 3-1. The bronchi were extended and connected with 8 silicone tubes diameter of 2 mm, and 31 silicone tubes diameter of 1 mm. The trachea end has non-circular profile, therefore a converter made of silicone cast and 3D printed plaster (Zprinter 250; 3Dsystems, South Carolina, USA) was constructed that gradually converts the cross sectional area into a circle with diameter of 9 mm. The end of the profile converter has an outer diameter of 16 mm and is connected to a 16 mm inner diameter rubber hose.

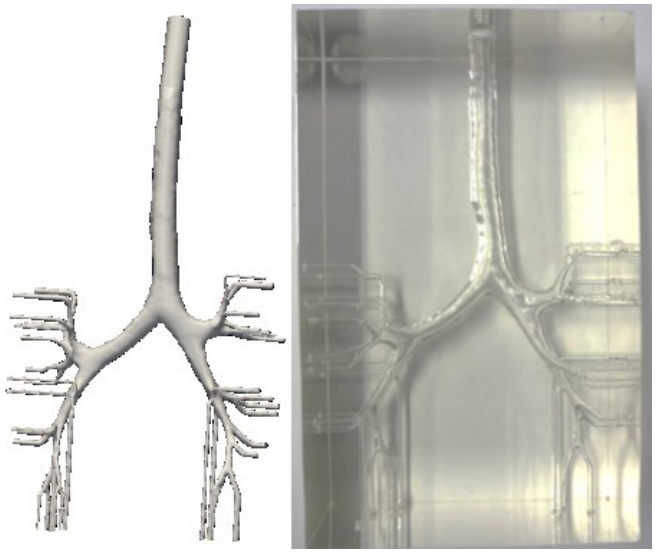

Figure 3-1. (Left) The reconstructed surface image of the lung airways. The bronchus ends were extended to accommodate the flow in the experiments. (Right) The silicone model used in the acoustic pressure visualization.

The experiments performed by measuring the sound generated by air flowing through the silicone model at inspiration and expiration maneuver. The air supply system consists of a compressor (Kapsel-con YC-4RS; Hohmi, Japan), an air tank (Anest Iwata SAT-120C-140l Anest Iwata Corp., Japan), a flow controller (Azbil MQV0050B, Azbil Corp., Japan), and a 16

mm inner diameter rubber hose as shown in Figure 3-2. Air at room temperature flows from the compressor to the air tank until the pressure inside the air tank reach 0.5 MPa. This filled-air tank is used at the measurement time so there is no compressor noise when the acoustic measurements were performed. Before entering the silicone model, the air flow from the air tank to a flow controller, which control a constant flow with flowrate of 500 $mL.s^{-1}$, and then to an acrylic cylinder with sponge and honeycomb-like structure to reduce the flow fluctuation and generate a laminar flow. In representing the inspiratory flow, the air entered from the acrylic cylinder to the silicone model from the trachea flow converter, while in the expiratory flow, the air from a main acrylic cylinder separated into four other acrylic cylinders before entering the bronchi ends through silicone tubes. The flow rate of 500 $mL.s^{-1}$ was used in both expiration and inspiration case which corresponds to a Reynolds number of 4800 calculated at the trachea region for the peak of the tidal volume breathing. This flow rate is smaller compared to the flowrate used in other study such as in [15], [37] to accommodate the smaller lung due to the age of our subject. The silicone model and the flow divider were put inside an anechoic room (size: 90×90×92 cm^3) and all noise-generating equipments were located outside when measurements were performed. The outlet was also extended and inserted to an anechoic expansion box to diminish the outlet sound. Leakage test was performed in every measurement by locating a flow meter at the outlet and ensuring the same flow rate at inlet and outlet.

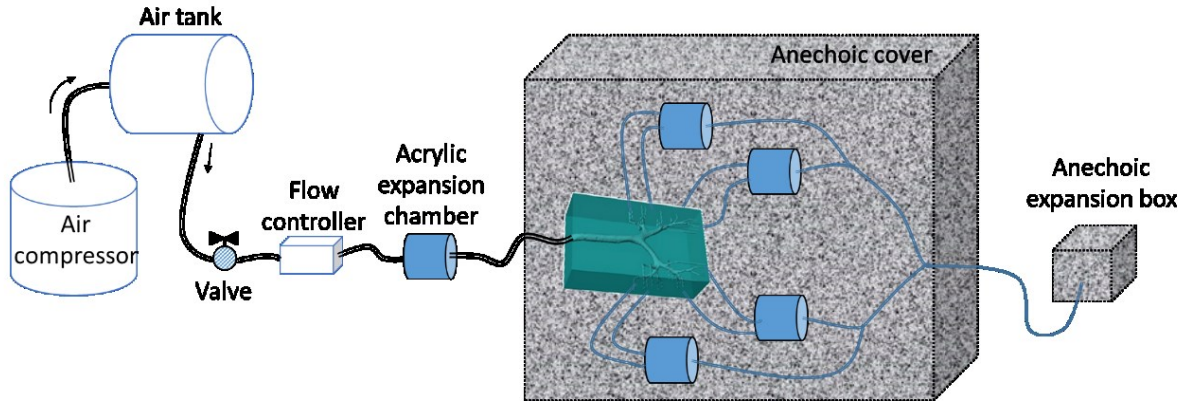

Figure 3-2. The flow supply configuration used in the experimental setup.

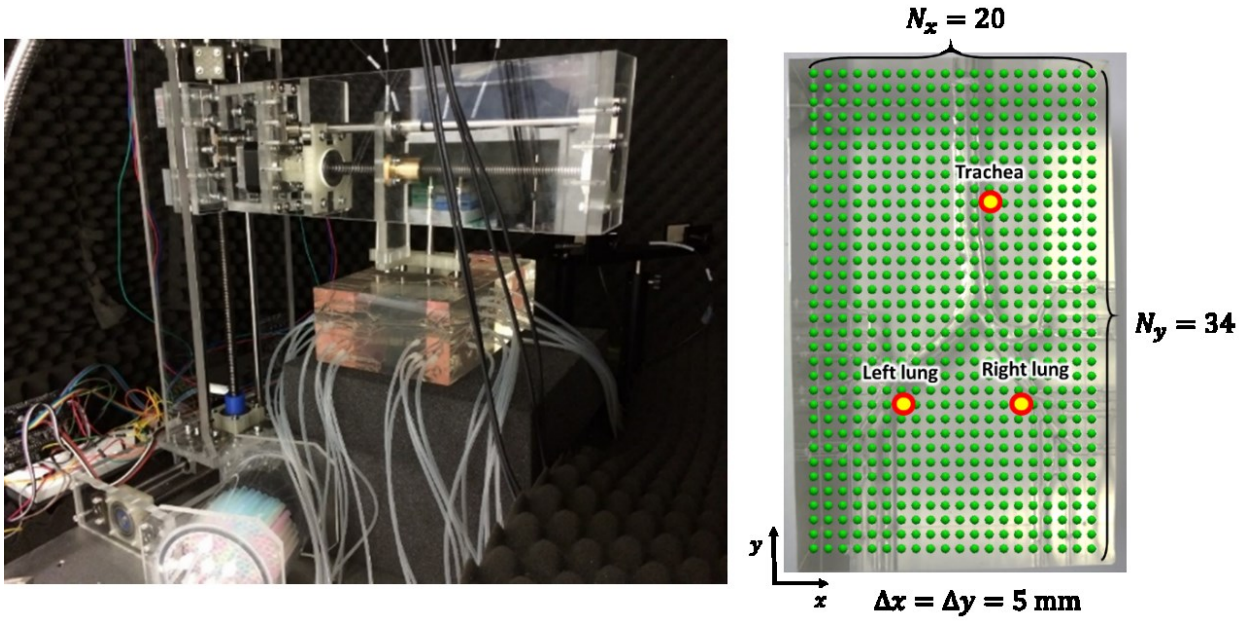

Figure 3-3. (Left) The microphone array system connected to automated stage to measure the sound pressure field. All outlets of the silicone model were connected to silicone tube and extended to outside of the anechoic room to prevent outlet noise. (Right) The sound measurement locations contains of 20 points in *x*-direction, 34 points in *y*-direction with distance of 5 mm between each measurement points. In total, pressure field of 680 points were gathered. Yellow points indicate the location of the sampling point location for Figure 3-4.

A microphone array system consists of four free field array microphone (G.R.A.S. 40PH, G.R.A.S. Sound and Vibration A/S, Denmark) with a programmable automatic 3D moving system using Arduino microcontroller was used to scan the sound pressure field over the silicone model. All microphones were calibrated to a class 1 pistonphone calibrator (RION Sound Calibrator NC-74, RION Co. Ltd., Japan) to ensure the same reference pressure for all microphones. These microphones recorded the sound pressure at a distance of 2-3 mm between the microphone tip and the silicone model surface for every 5 mm in horizontal and vertical direction as shown in Figure 3-3. In total, current setup can achieve 680 measurement locations covering the area of 95×165 mm^2. The measurements data were digitized using a National Instruments data acquisition NI PXIe-4492 (National Instruments Corp., Texas, USA). Each

measurement contains of 5 seconds pressure data with sampling frequency of 20,000 Hz and 16 bit depth. The 2048 points Fast Fourier Transform (FFT) with Hanning window was applied to the sound pressure data with an overlapping ratio of 0.5 to obtain the average sound spectra using MATLAB R2015a (MathWorks, Inc., USA). To characterize the sound, the OASPL was calculated following equation 2-1. In current measurement, the OASPL calculation was performed for frequencies between 900-5000 Hz as the signal to noise ratio was poor below 900 Hz and above 5000 Hz.

3.3. RESULTS

Sound spectra of three different sampling points at the trachea region, left lung, and right lung (refer to Figure 3-3) at inspiration and expiration direction are shown in Figure 3-4. The comparison with the background noise shows wide band increase at frequencies between 1000-2500 Hz for inspiration with several peaks between 3500 Hz and 4000 Hz and between 1000-4000 Hz for expiration. In both inspiration and expiration, the trachea measurement point shows a slightly higher PSD at lower frequency compared to other points. It can also be seen that among the three measurement points, the inspiration case generates higher PSD compared to the expiration case, especially at the trachea measurement in the frequencies less than 1500 Hz.

The overall sound pressure level between 900-5000 Hz is shown in Figure 3-5. From this plot, we can roughly see the shape of the airway geometry based on the calculated OASPL. The maximum OASPL are higher in expiration rather than in inspiration direction. The maximum OASPLs are located on the trachea region for the inspiration case, and on the left and right branch for the expiration case. An asymmetry pattern of the OASPL distribution was

also found with right upper part are showing a higher value of the OASPL compared to other part.

Figure 3-6 shows the color-graph of the sound PSD distribution for all measurement points at some arbitrary frequencies. At inspiration, low frequency sound components can be observed for at the trachea region. Small level of the high frequency components are found at the small airway region. At expiration, the sounds distributed from the trachea to the small airways. At the trachea, the generated sound tends to have low frequency components, while at the small airways, the sound tends to have high frequency components in a significantly higher level than those in the inspiration case.

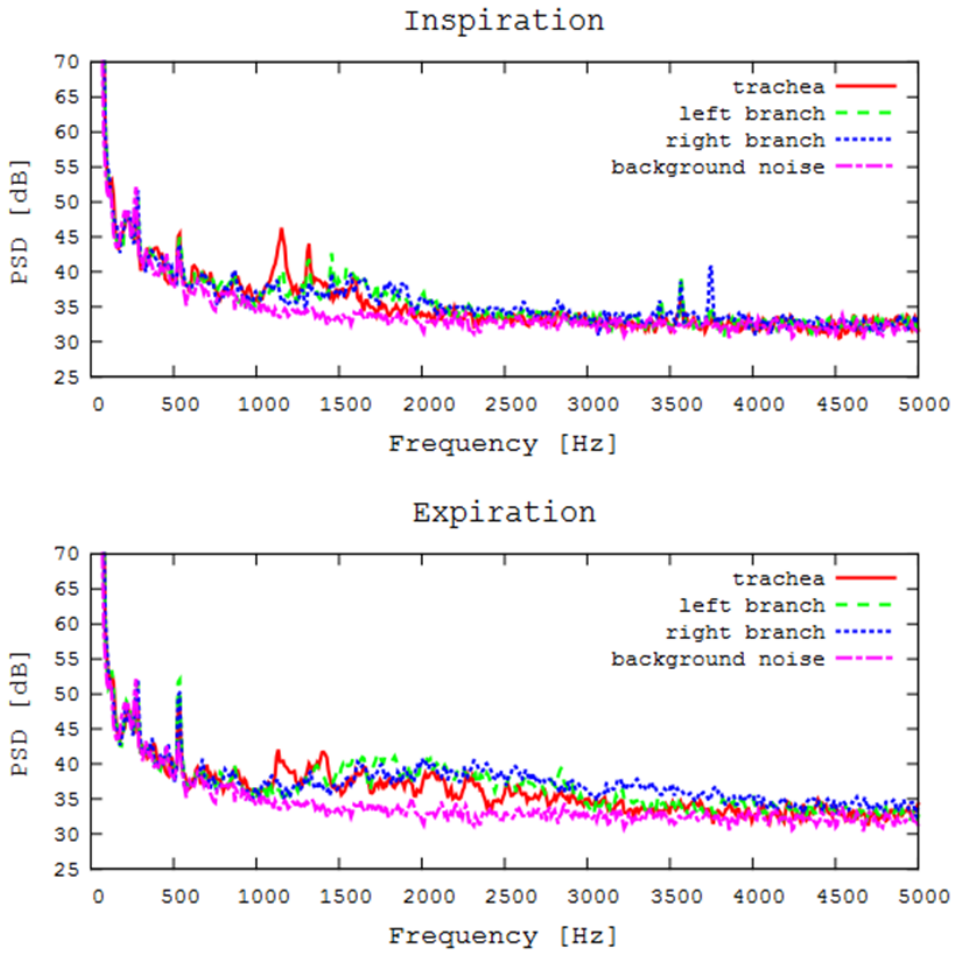

Figure 3-4. PSD of the inspiration (top) and expiration (bottom) measured above trachea, left branch, and right branch on the silicone airway model indicated in Figure 3-3. Background noise were presented as comparison.

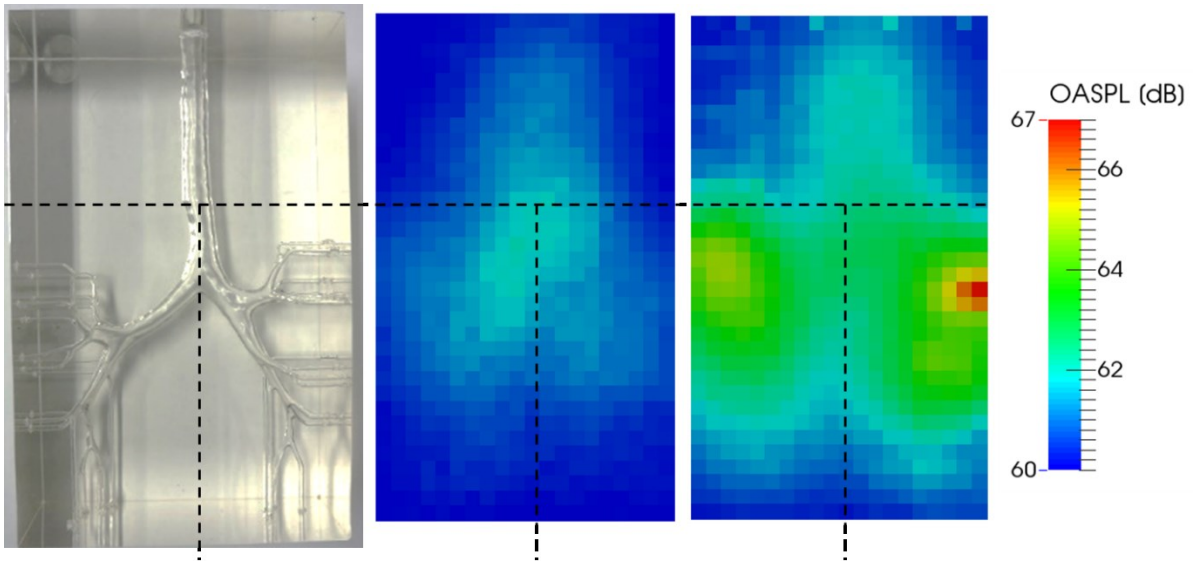

Figure 3-5. Overall sound pressure level for all measurement points in a color contour plot for inspiration (center) and expiration (right). Dashed line are shown to indicate the same location on the silicone model.

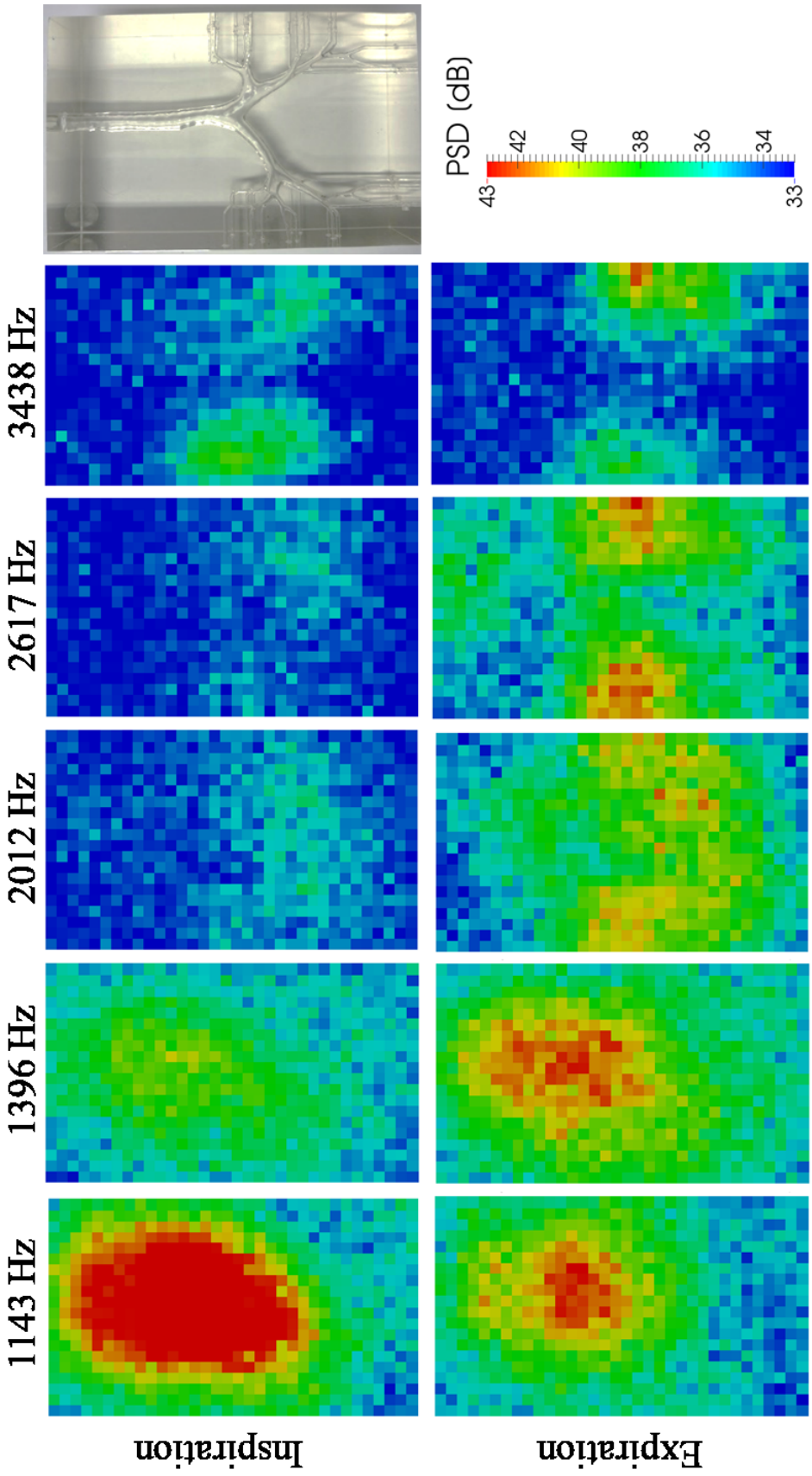

Figure 3-6. PSD distribution at some sampled frequencies.

3.4. DISCUSSION

The identification of source location and characteristics of the sound generated aerodynamically by air flow in tracheobronchial geometry is required in order to provide comprehensive analysis of respiratory diagnosis. Current results show the ability to map the sound characteristics of 680 measurement points on the surface of the silicone airway model. In our results, an increase of PSD level was found in the lower frequency range at trachea and first branch region on both expiration and inspiration case. At small branches, the frequency was more likely to be higher than 2000 Hz and was distributed widely over the left and right lungs. The frequency was more apparent in the expiration case.

Our results also found that wide frequency sound were generated during expiration and inspiration. The range itself is considered to have a wider range compared to those found in [12], [15], [90], [91] which is measured on the chest surface. This indicated that the original sound generated aerodynamically in the bronchial airways originally has a wider frequency range compared to those measured on the chest surface. The complexity of the lung tissues, skin, chest bone, etc. may result in the reduction of the higher frequency component which needs further investigation.

The sound distribution and characteristics may be related to different sound generation mechanisms and the resonance characteristics of the geometry. According to the results obtained in Chapter 2, we observed that the sound frequency distribution measured by a model is relatively constant instead of the flow rates. This condition may indicate that the sound generated in each measurement location will be relatively constant and will depend only on the geometry of the airway in the silicone. However, a certain flow condition is required to generate the sound.

Inspiration and expiration maneuver tend to generate a wide band sound frequency, which has different range point by point. It is still not clear what causes the differences of the

frequency distribution in the expiration and inspiration. One of the possible reasons is that the direction of the flow changes the flow disturbance characteristics. The inspiration direction was observed to generate only the low frequency component of the sound and it may indicate that the flow disturbance only occurs in trachea and main bronchus region. The flow disturbance attenuates as the airway is getting smaller and no more flow disturbance is found in the small airway. In the expiration direction, flow disturbance was generated by the geometry itself and was high enough to generate the high frequency component in the small airways. The flow disturbance in the small airways continued and was accumulated in the main bronchus and trachea region, which lead to the generation of low frequency component.

The asymmetry distribution found in our study is similar to one that was found by Pasterkamp [91] where the average power at low (100-300 Hz), medium (300-600 Hz), and high (600-1200 Hz) were calculated for the sound measured on the chest surface. A higher level of sound power on the right upper anterior lung was also observed in the measurement of adult. However, the distribution of the inspiration was higher in the right lung compared to the left lung. This difference may be caused by different calculation method and frequency range used for calculating the average value of the sound power.

3.5. SUMMARY

An effort to identify the sound source location and characteristics generated by air flowing in a tracheobronchial geometry is presented in this chapter. A total of 680 measurement points data were collected and map to show the distribution of the sound source for each frequency. In the inspiration maneuver, the frequency tends to distribute in the low frequency region of less than 1500 Hz and small parts in the frequency higher than 2000 Hz. In the expiratory direction, a wide band frequency sound was observed in the range of 1000-4000 Hz. The map

of the power spectral density distribution indicates that in the source of the sound with frequency less than 1500 Hz are located in the trachea region. While the source of the sound with frequency higher than 2000 Hz is located in the small airway branch. This frequency distribution is similar in the inspiration and expiration maneuver, however, high frequency component is more noticeable and more consistent in the expiration. This leads to a significant increase in the overall sound pressure level (OASPL) in the small airway region for expiration case.

Chapter 4

Fluid flow simulation of the airway model

4.1. INTRODUCTION

In the previous chapter, the sound sources for each frequencies were detected by using the microphone array and silicone lung airway model. Computational fluid dynamics (CFD) simulations are performed in this chapter in order to describe the flow condition lying behind the generation process of the aerodynamic sound in the tracheobronchial model.

Computational fluid dynamic simulation is recognized as a powerful method to analyze the flow condition especially in a complex geometry such as the tracheobronchial system. Simulations of the respiratory flow can be found mainly in the study of respiratory flow pattern [64], [92]–[95] or in the study of particle deposition [27], [30], [31], [35], [93], [96], [97]. CFD enables us to observe a local characteristics of the flow such as the particle deposition and the sound source terms which is difficult to be measured experimentally. In this chapter, a CFD analysis of incompressible fluid in the tracheobronchial geometry was introduced. The sound source terms described by the Lighthill source terms are calculated and the frequency characteristics of the sound source terms were calculated to explain the frequency dependencies found in Chapter 3.

4.2. METHOD

Simulations of the flow inside the airway in both direction, inspiration and expiration, were performed in this study. Incompressible Newtonian fluid is assumed to characterize the fluid. The Large Eddy Simulation (LES) technique with dynamic Smagorinsky-Lilly model [98] is applied in order to evaluate the sub-grid scale stress. The governing equations of the fluid solver

are determined by the spatially-filtered incompressible continuity equation and momentum equation given by

$$\nabla \cdot \bar{\mathbf{u}} = 0, \qquad \text{(eq. 4-3)}$$

$$\frac{\partial \bar{\mathbf{u}}}{\partial t} + \nabla \cdot (\bar{\mathbf{u}}\bar{\mathbf{u}}) - \nabla \cdot (\nu \nabla \bar{\mathbf{u}}) = -\nabla \bar{p} + \tau_{SGS}. \qquad \text{(eq. 4-4)}$$

Here, $\bar{\mathbf{u}}$ is the filtered velocity vector, ν is the kinematic viscosity, $\bar{p}$ is the filtered pressure normalized to the density of the fluid, and τ_{SGS} is the unresolved sub-grid-scale stress. The flow simulations are solved on an open-source fluid solver platform OpenFOAM 2.3.0 with the PISO (Pressure Implicit with Splitting of Operator) algorithm. Here, the residual values of 1×10^{-9} is used as a convergence criterion for both velocity and pressure.

A tetrahedral mesh with prism boundary layers configuration based on the silicone airway geometry is constructed using ANSYS ICEM CFD 13.0 (ANSYS, Inc., Pennsylvania, USA). In total, 6,747,430 volume mesh and 2,148,421 points are used for the calculations. The mesh domain is constructed using adaptive mesh construction (Figure 4-1) to tackle the minimum number of mesh in each cross-sectional area of the large and small bronchi. Each boundary condition, consist of a trachea, 39 bronchus, and the airway wall, is defined separately (refer to Appendix B for the detail location of each boundary).

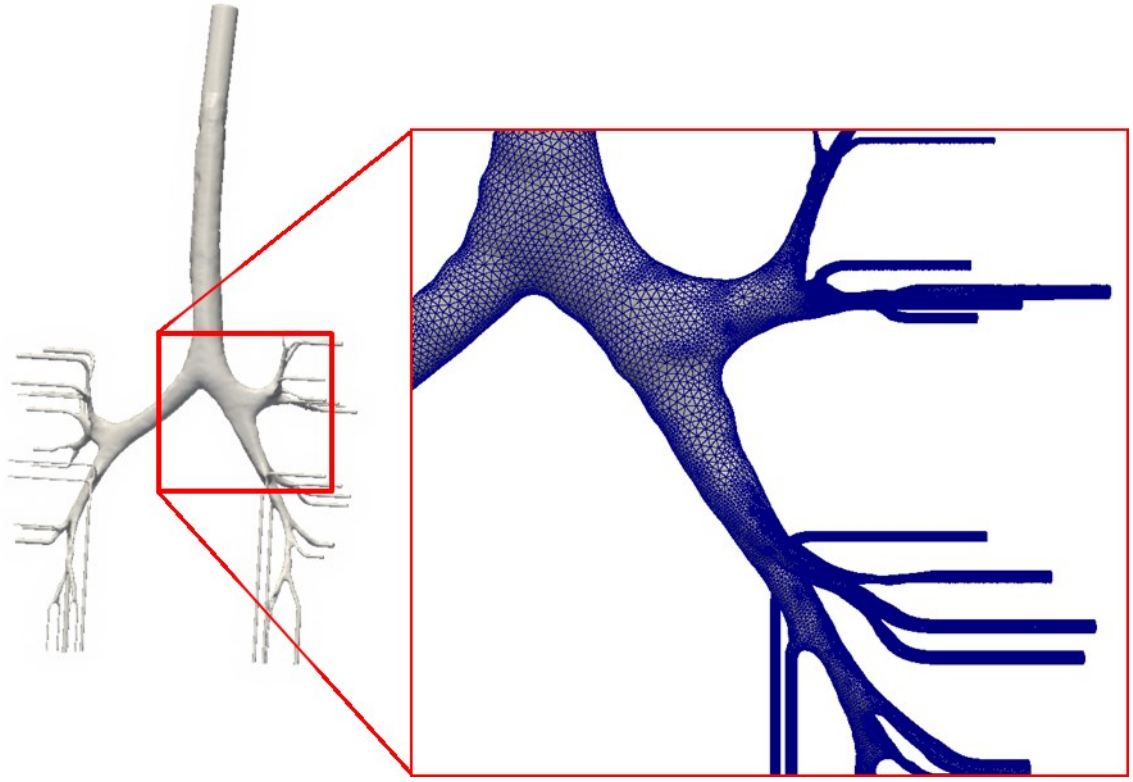

Figure 4-1. Adaptive mesh configuration used in the CFD.

Inspiration case is represented by defining the trachea as constant velocity inlet with a uniform 7.2 $m.s^{-1}$ velocity profile with zero pressure gradient. The bronchus ends are defined as a constant zero pressure outlet and zero gradient velocity value. This condition is valid based on the assumption of the isotropic expansion of the lung at the peak of inspiration maneuver with 495 $mL.s^{-1}$ flowrate which corresponds to the Reynolds number of 4800. This value is similar to the value used in the experimental measurement of the acoustic visualization in Chapter 2.

In the expiration case, a constant velocity inlet is imposed on all bronchus ends while the zero pressure outlet is imposed at the trachea. The velocity profile at the each bronchus end is determined based on the results of the inspiration case. This lets us to simulate the different velocity of each bronchus which based on the respective volume of the alveolar sacs. The airway wall is defined as non-slip wall conditions in all simulations.

The simulations were performed with a calculation time step increment of 1×10^{-7} s up to 0.029 s. The data from 0.016 s to 0.029 s with a step of 5×10^{-5} s were used to calculate the mean velocity and the root mean squared (RMS) velocity fluctuation. The sound source term of the incompressible fluid based on Lighthill acoustic analogy was also calculated in this time range. The Lighthill acoustic analogy is defined by

$$\left(\frac{1}{c_p^2}\frac{\partial^2}{\partial t^2} - \nabla^2\right)\left[c_p^2(\rho - \rho_0)\right] = \nabla\cdot\nabla\cdot\boldsymbol{\tau} \qquad \text{(eq. 4-4)}$$

where c_p is the sound speed in the reference fluid, ρ_0 is the reference fluid density, ρ is the fluid density, and $\boldsymbol{\tau}$ is the reduced form of the Lighthill stress tensor which is described by

$$\boldsymbol{\tau} = \rho\overline{\mathbf{u}'}\overline{\mathbf{u}'}. \qquad \text{(eq. 4-5)}$$

We will not use the full Lighthill acoustic analogy show in eq. 4-4 to solve the acoustic propagation in current study. Only the right hand side of the Lighthill acoustic analogy (eq. 4-5), which is considered to be the source term for the acoustic propagation, is calculated. The frequency distribution of the sound source term was also calculated by using the 128 points Fast-Fourier Transform of the divergence of the Lighthill tensor for 5 data sets with 0.8 overlapping coefficients.

4.3. RESULTS

The flow distribution for each bronchi end based on the results of the inspiration maneuver simulation is shown in Table 4-1. This distribution is described in the terms of the maximum mean velocity magnitude, maximum velocity RMS magnitude, and the flow rate for each bronchi. This distribution profile is used as the inlet value for the expiration simulation. Please refer to Appendix B for the definition and the location of each bronchus name. A maximum value of mean velocity magnitude can be observed in bronchi 26 and 33 with a value of 30.3 $m.s^{-1}$, while the maximum RMS can be observed in bronchi 24 with a value of 1.907 $m.s^{-1}$.

Table 4-1. Flow distribution obtained from inspiration simulation*.

Boundary label	Maximum mean velocity [m.s-1]	Maximum RMS velocity [m.s-1]	Flow rate [mL.s-1]
Trachea	7.2 (9.46 at expiration)	0 (0.98 at expiration)	495
Bronchi 1	20.6	0.358	27.4
Bronchi 2	21.7	0.139	12.5
Bronchi 3	14.1	0.026	2.14
Bronchi 4	16.4	0.452	22.7
Bronchi 5	23.9	0.313	14.1
Bronchi 6	24.3	0.238	15.3
Bronchi 7	14.9	0.039	2.29
Bronchi 8	10.9	0.007	1.62
Bronchi 9	9	0.008	1.32
Bronchi1 0	8.3	0.148	3.98
Bronchi 11	21.5	0.056	3.31
Bronchi 12	29.6	0.714	40.3
Bronchi 13	22.2	0.466	13.8
Bronchi 14	18	0.018	2.8
Bronchi 15	19.6	0.021	2.97
Bronchi 16	17.5	0.029	2.67
Bronchi 17	19.5	0.023	3
Bronchi 18	16.8	0.021	9.31
Bronchi 19	26.1	0.625	32.5
Bronchi 20	16.1	0.054	8.82
Bronchi 21	14.1	0.842	8.35
Bronchi 22	14.6	0.315	2.18
Bronchi 23	22.1	0.021	12.4
Bronchi 24	23.2	1.907**	29.7
Bronchi 25	25.8	0.212	16
Bronchi 26	30.3**	1.468	43.5**
Bronchi 27	21.4	0.123	13.4
Bronchi 28	25.7	0.212	15.8
Bronchi 29	23	0.127	14.1
Bronchi 30	24.8	1.482	14.7
Bronchi 31	27.3	0.402	17.3
Bronchi 32	20.1	0.033	3.1
Bronchi 33	30.3**	0.431	18
Bronchi 34	26	0.675	34.2
Bronchi 35	10.5	0.091	5.12
Bronchi 36	26.5	0.742	16.4
Bronchi 37	20.7	0.04	3.22
Bronchi 38	9.5	0.024	1.38
Bronchi 39	21.7	0.027	3.3

All values are obtained from inspiration maneuver unless stated elsewhere.
(*) Refer to Appendix B for the definition and location of each Bronchi name.
(**) The maximum value of each category.

The mean velocity magnitude and the RMS of the velocity at the center plane of the trachea and main bronchus region for inspiration and expiration are shown in Figure 4-2 and Figure 4-3 respectively. On this cross sectional plane, in the inspiration direction, a relatively uniform velocity field can be observed in the trachea region. The inertial force of the flow makes the high speed flow from the trachea attach to the distal part of the right and left main bronchus. This similar pattern caused by the inertial force can be found in almost all branching point. In the expiration direction, the maximum mean velocity can be found in the meeting point of two branches. We can clearly notice a high velocity flow field in the distal part of the trachea, and the distal region of the main branches where the flow from the small airways meet.

The RMS of the flow velocity shown in Figure 4-3 shows the location of the high fluctuation in the bronchial model. A slightly higher of RMS value can be seen from the darker red colored area in this image. For the inspiration case, higher RMS value can be found in the location of the outer side of the main branch, and the branching wall where the flow impinge before separated to the daughter branches. High RMS value in the expiration direction can be observed in the region of the meeting point of two branch. It is also noted that high RMS region in expiration case can be found also in the side wall area where the flow from the bronchi impinge before entering the larger airways.

The value of sound source terms of the Lighthill acoustic analogy defined by the divergence-divergence of the Lighthill stress tensor is shown in Figure 4-4. A similar pattern to the one observed from the RMS value can be found on this image. A red-blue region indicating a low-high value of the sound source term can be observed in almost all meeting point of the branch at expiration case. This high value also significant in the small airways region, and the center of the meeting point of the main bronchus. In the inspiration case, the sound source term value is not as high as those found in the expiration case. High value of the

sound source term in the inspiration direction can be found in the side wall of the branch and the location of the flow impingement.

The frequency dependencies of the Lighthill sound source terms are shown in Figure 4-5. In the lower frequency case, a high level of PSD can be observed at all parts of the trachea and main bronchus at expiration direction and only at the branching location after the left and right main bronchus. Both in the expiration and inspiration cases, the level of PSDs in almost all locations is decreasing as the frequency increases. However, in the expiration case, we still can observe PSD of more than 125 dB in the main bronchus region at frequency of 5000 Hz. As for inspiration case, the level of the PSDs is much reduced and only low level of PSD can be observed in the same location with the low frequency sound source term.

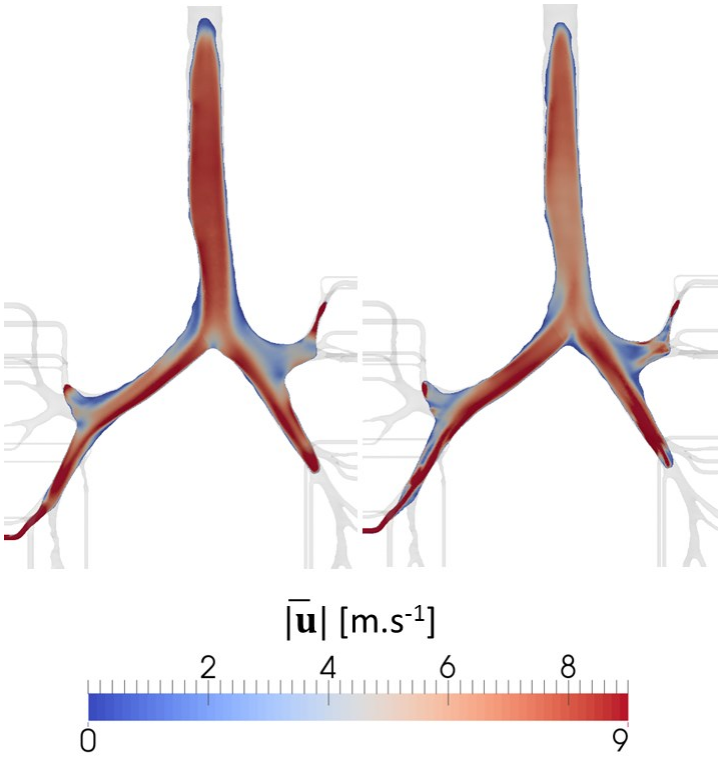

Figure 4-2. The color contour of the mean velocity magnitude of at inspiration (left) and expiration (right).

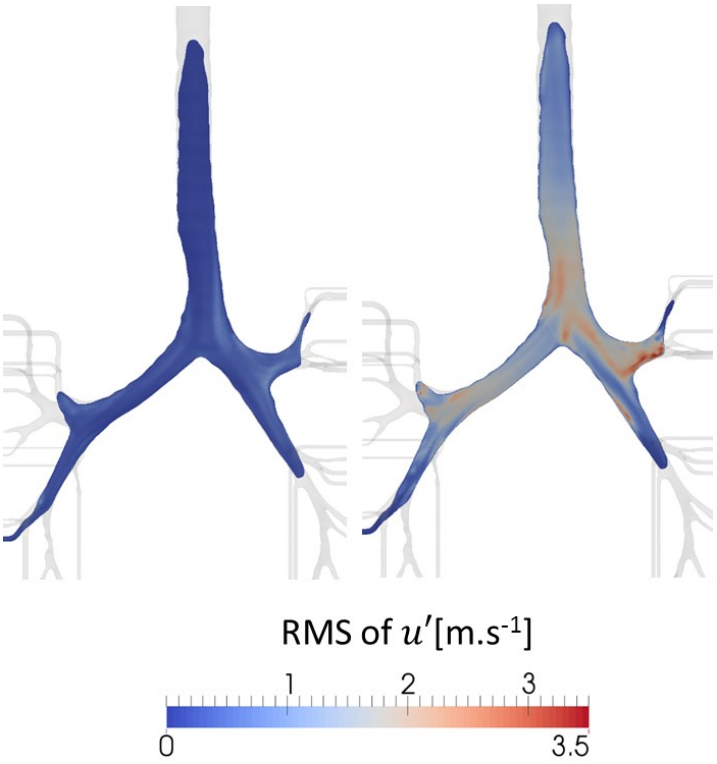

Figure 4-3. The color contour of the root mean squared magnitude of the fluctuating velocity component at inspiration (left) and expiration (right).

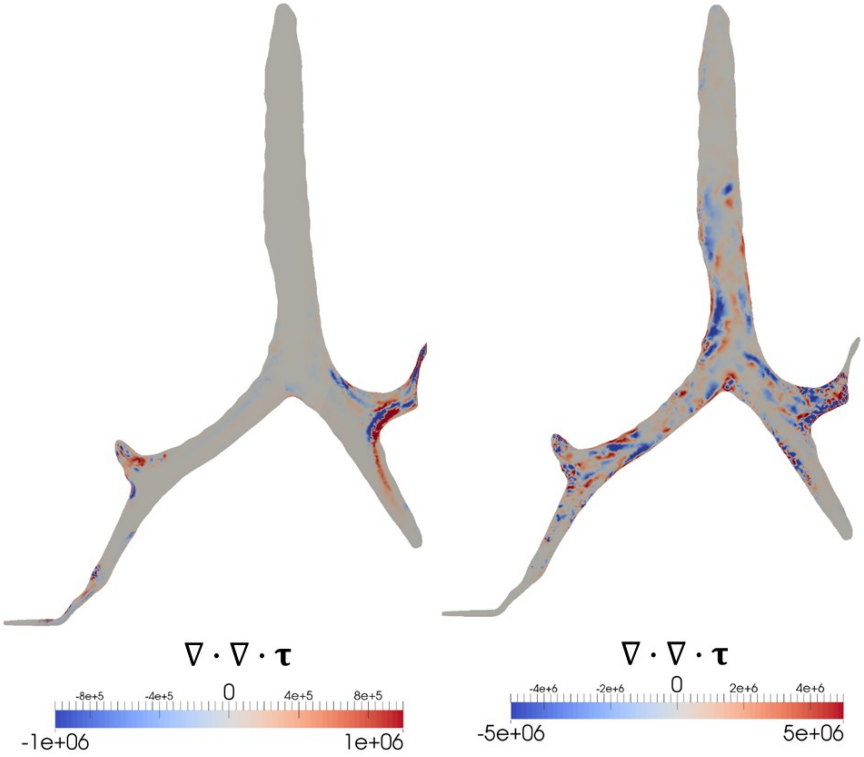

Figure 4-4. Instantaneous value of the source terms of the Lighthill acoustic analogy or the divergence-divergence of the Lighthill stress tensor at t=0.029 s for inspiration case (left), expiration case (right).

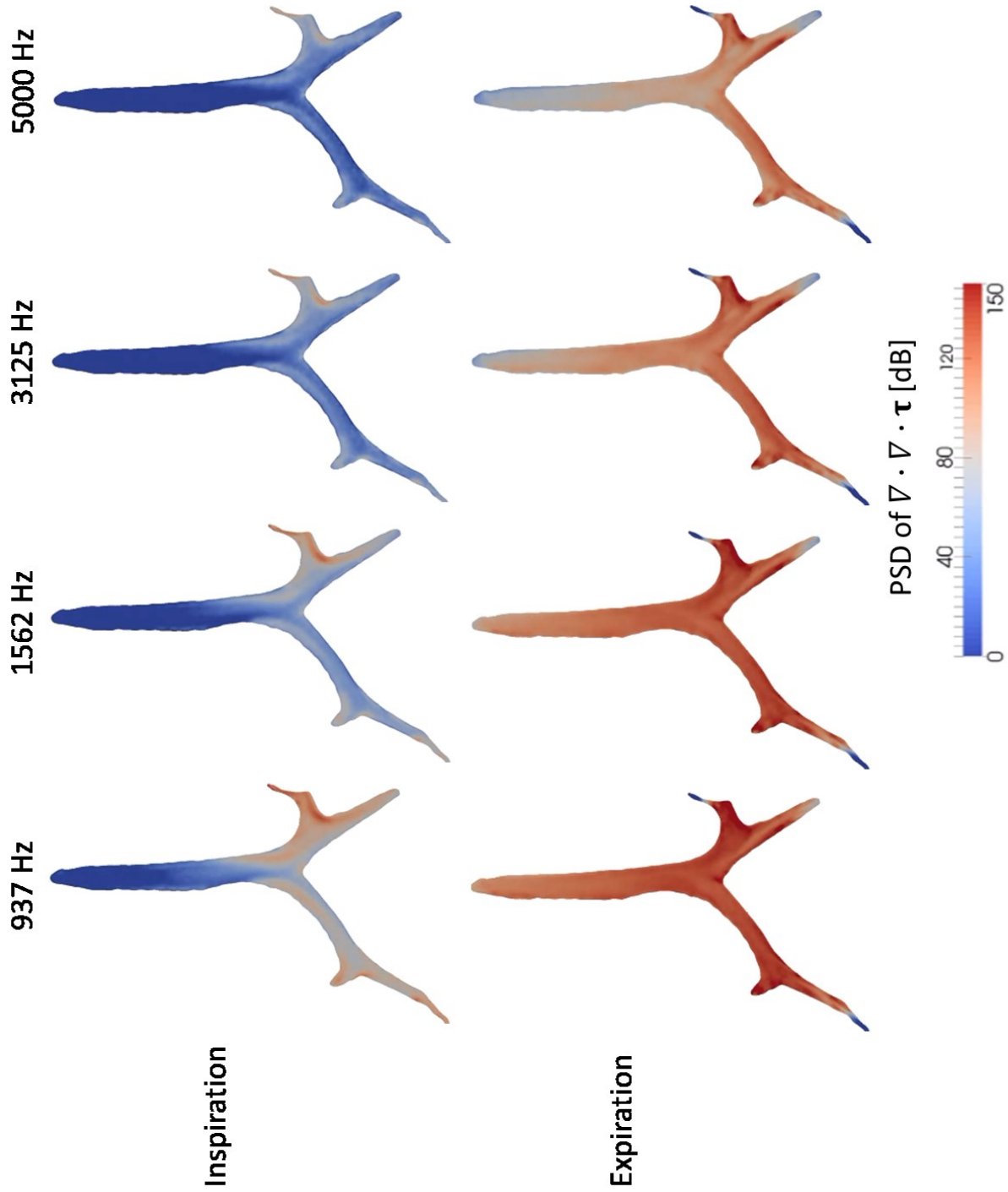

Figure 4-5. The PSD of the Lighthill sound source terms at several frequencies.

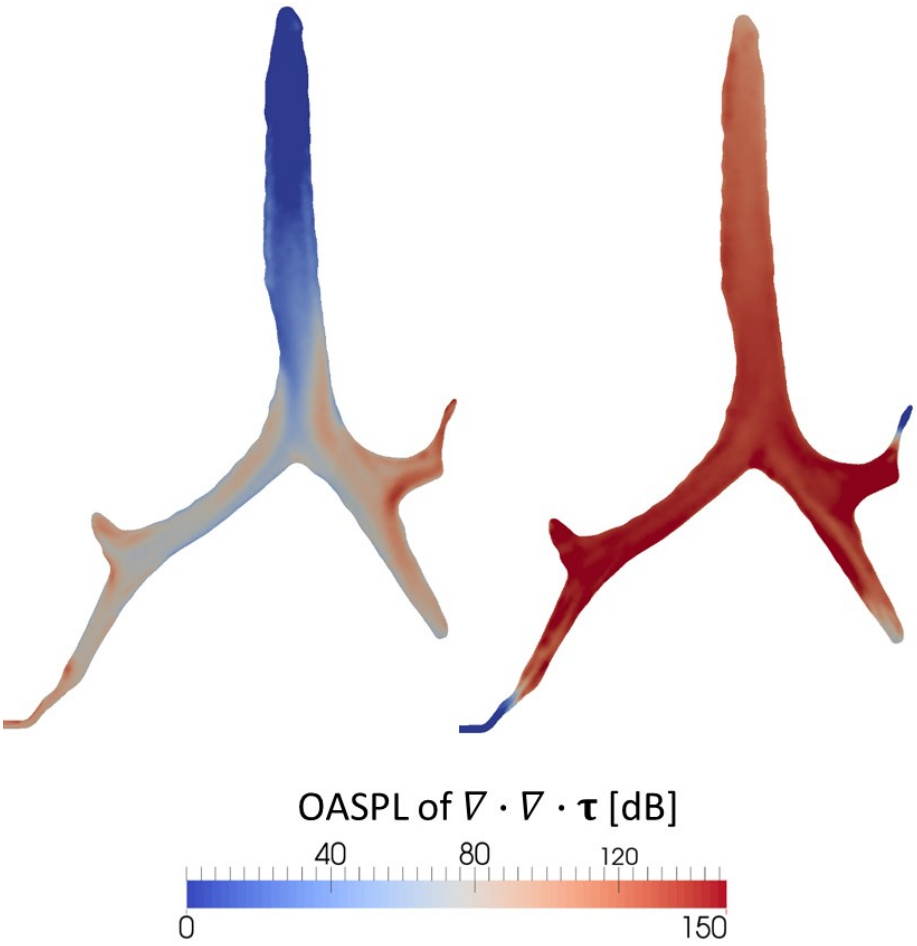

Figure 4-6. OASPL of the Lighthill sound source term for frequency range of 900-5000 Hz at inspiration case (left), and expiration case (right).

4.4. DISCUSSION

The distribution of the sound source terms based on the computational fluid simulations is calculated. The mean and RMS of the velocity shown in Figure 4-2 and Figure 4-3 show the initial prediction of the location of the fluctuation in the tracheobronchial geometry. Velocity fluctuation is commonly related to the disturbance, which causes the pressure fluctuation and sound.

The complexity of tracheobronchial geometry is considered to be one of the important factors contributing to velocity fluctuation. The RMS distribution shown in Figure 4-3 describes different locations of the velocity fluctuation in expiration and inspiration maneuver.

In inspiration case, a uniform velocity field is imposed at the trachea. In current model, the flow velocity at the center region of the trachea is higher compared to the velocity at the outer region creating a Poiseuille flow-like velocity profile. High flow velocity impinges the first branching point and splits to the main left and right bronchus. However, the inertial force of the flow causes the flow to attach to the distal part of the branch. This creates a low-pressure region at the side-region of the branch and generating a small region with reversed flow which commonly named as flow separation. This flow separation creates a fluctuating velocity region indicated by higher RMS value at the right and the left side of the trachea rather than the central region. In addition, the flow at the central region of the airways impinges the edge part of the branching point creating an unstable-stagnation point, which also contributes to the velocity fluctuation. These flow separation and unstable-stagnation flow impingement can be found in almost all branching locations with different magnitudes. In the Table 4-1, we can observe the maximum RMS at bronchi 24 which is located at the distal parts of the model (refer to Appendix B for the detailed location) and has a difference of 9 generation branching to the trachea. It may indicate that the flow disturbance caused by the branching configuration can continue or propagate up to the small airways.

In expiration case, the inlet velocity of each bronchi is asymmetric and ranges from as low as 9 $m.s^{-1}$ to as high as 30.3 m.s-1 as shown in Table 4-1. This high velocity yet asymmetric flow collides to each other in the branching locations and generates a vortex pattern which is known to be able to generate sounds [99]. The flow collision in the branching locations also creates a low pressure region at the outer region of the meeting point which induces the flow separation and fluctuation indicated by the high RMS value at the outer side of the meeting points of each branches.

The Lighthill sound source terms are calculated to observe the locations of the sound source terms and the frequency dependencies of the sound sources. The high intensity of the

instantaneous Lighthill source terms shown in dark blue and dark red region in Figure 4-4 indicates the location of the quadrupole sources generated by the turbulence or the chaotic flow. The high intensity sound sources indicate a similar location to those found in RMS calculations.

Figure 4-5 shows the frequency dependencies of Lighthill sound source terms. Here, we observe a clear dependency of the sound source terms to the frequency especially in trachea region. The sound pressure level in trachea region will decrease as the frequency increases in both case of inspiration and expiration. This tendency was also found from the measurement results explained in Chapter 3. Comparing the PSDs on the trachea region, we observed broader and higher PSD values on inspiration direction compared to those in expiration direction based on the measurement results in Chapter 3. Nevertheless, the PSD of inspiration is slightly lower compared to the PSD of expiration in trachea region based on the numerical simulation results. These different characteristics can be explained by different inlet condition applied in the trachea region. In our numerical simulation, a uniform velocity field was implied on the trachea which might be not enough to represent the realistic boundary condition in the silicone tracheobronchial model. Furthermore, the inlet converter at the trachea used in the experiments, might induce artificial turbulence at the trachea which induced to additional sound sources.

In small airway region, the sound source terms show a relatively constant value in all frequencies which was also similar to the tendency found in the measurements. In expiratory maneuver, the PSD levels are higher in small airways rather than trachea region in both simulations and experiments. This may indicate that collision of high flow velocity coming from each bronchi tends to generate higher frequency sounds with larger amplitude compared to the collision of low velocity flow found in the main bronchus and trachea region. This high frequency tendency is related to the small eddies generated in small airways, while low frequency component may be related to the large eddies generated such as found in trachea region.

The OASPL of the PSDs calculated from the Lighthill sound source terms for the expiration case shows a similar tendency to the OASPL pattern obtained in experimental measurements. However, the OASPL for inspiration shows a slightly different patterns which may be caused by the inlet condition of the experimental setup.

4.5. SUMMARY

An effort to explain the flow condition related to the sound generated aerodynamically in the tracheobronchial model was performed by using computational fluid simulation. Applying the Lighthill acoustic analogy, the locations of the sound sources and the frequency dependencies of the sound sources were observed. Similarly to the results obtained in Chapter 2, the sound in the trachea region has lower frequency characteristics compared to the sound observed in the small airways. The sound sources of the expiration are located in the outer side of a branching point and the near wall region where flow attachment appears as a results of the high velocity flow. In the inspiration case, the sound sources are located at the sides of the branching points where the area expansion leads to a flow separation and the location of the flow impingement as the results of the inertial forces. It can be concluded that in the expiration case, flow collision, flow impingement, and flow separation are contributing to the flow disturbance which generates the sound. While flow impingement and flow separation are the main mechanisms contributing to the sound generation in the inspiration maneuver.

Chapter 5

General Conclusion

In this study, experimental and computational studies were performed in order to reveal the sound generation mechanisms in the respiratory flow using simplified model and realistic tracheobronchial model based on aerodynamic sound generation theory. The measurement of sound and flow fluctuation in the T-branch model reveals the combination of the flow rate and the constriction, which in results change the Reynolds number, may show the requirement of the flow condition to generate the sound. It was found that a flow with Reynolds number more than 4000 was substantial to initiate a 2 dB sound. The occurrence of the flow condition in the respiratory airway may also generate the sound in the same pattern. To explain the sound generation behavior and the source location in the respiratory airway, we employed a realistic model to detect the source accurately.

The sound generated aerodynamically by the flow in the CT-image based lung airway model was studied experimentally and computationally. The acoustic sound pressure near the surface of the silicone model was compared to the RMS of the velocity fluctuation from the CFD simulations. The sound generated by the fluid flow or commonly called aerodynamic sound can be correlated to the fluctuation of the velocity or pressure that appear when a fluid move over a solid boundary or by flow instability [100]. The measurement of the pressure field at 680 points on the silicone surface enabled us to map the acoustic pressure sound density on surface of the silicone model. This method let us to observe the location of the source in the airway. In our results, an increase PSD level was found in the lower frequency range at the trachea and first branch region on both expiration and inspiration case. At the small branches, the frequency tends to be higher and distributed widely over the left and right lungs. This results may indicate a different sound generation in this model.

The CFD simulations were used to explain the sound generation mechanisms at a flow rate 25% of the one used in the experiment. For the inspiration case, the mean velocity magnitude tends to increase from the trachea region to the small airways. This value increases up to the 8 $m.s^{-1}$ in current simulation. This result is in agreement with [65], however, this mean velocity will reduce further more in the physiological model caused by the increase of the total cross-sectional area of the bronchus. This phenomenon cannot be found in our model where the mean velocity continues to increase in some parts of the flow extension constructed to accommodate the outlet of the silicone model while not increasing its total cross-sectional area.

The fluctuation of the velocity which is represented by the RMS values in the CFD shown in Figure 4-3 reveals that large velocity fluctuation appears mainly branching regions. In the inspiration case, the fluctuation is generated at the flow separation region caused by the low pressure at the surrounding of the high speed velocity at the center of the airways and the flow impingement at the branching walls. This fluctuation can be found in almost all branching points and can proceed from the trachea up to bronchi end (e.g. bronchi 24 with the RMS value of 1.907 $m.s^{-1}$). While in the expiration case, the fluctuation starts to appear in the meeting points of two bronchi flows and the surrounding area. These fluctuations are high in all branching location indicated by red colored region in Figure 4-3. The calculation of the Lighthill sound source terms further supports this hypothesis.

Frequency calculation of the Lighthill sound source terms indicates that the strength of the sound source terms depends on the frequency. In the inspiration direction, the sound source terms of the sound less than 1000 Hz can be found on the main bronchus and the branching point at the small airways. We did not observe a high PSD values in the trachea region which may be caused by the inappropriate boundary conditions applied in the trachea and the initial turbulence in the experiment. However, a similar tendency can be observed for the frequency higher than 2000 Hz where the sound sources can only be found on the small airways.

For the expiration case, a good agreement between the experiment and simulation was achieved. The OASPLs of the simulation and the experiments are showing a similar pattern where strong sound sources are found in the small airway region and weak sound sources are found in the trachea region.

In summary, experimental and numerical efforts have been performed in this study to explain the sound generation phenomena in the human airway. Figure 5-1 may represents the general process of the aerodynamic sound generation in the tracheobronchial system. We found that main mechanisms contributing to the sound generations are different between the expiration and inspiration. In the inspiration case, flow impingement and flow separation are important to generate the sound, while in expiration case, flow separation and the collision of the high speed velocity flow from the bronchi have more contribution to the sound generation. It is also important to notice that the flow condition with Reynolds number of more than 4000 is required to generate an observable sound level.

In the case of a diseased lung, the initial condition of the disease may create a constriction in the airway region. This constriction leads to a higher Reynolds number since the patient will give more effort to obtain the same tidal volume flow rate. The constriction therefore increases the level of flow separation and flow impingement in the inspiratory direction, and increase the flow collision and separation in the expiratory direction which will generate a higher sound level measured on the chest surface.

It is important to notice that current results are valid for the case of the pure aerodynamically generated sound in the tracheobronchial geometry. The omission of the propagation behavior may simplify the study but cannot be directly applied to the real case of the respiratory sound. In the future, the A sound propagation simulation has also been prepared in order to accommodate the sound propagation characteristics in the silicone model and the respiratory systems. The integrated platform between sound generation and propagation can

support current findings to explain clearly the sound generated aerodynamically in tracheobronchial region and the propagation characteristics of the sound from the source through the multi-material environment in the chest cavity.

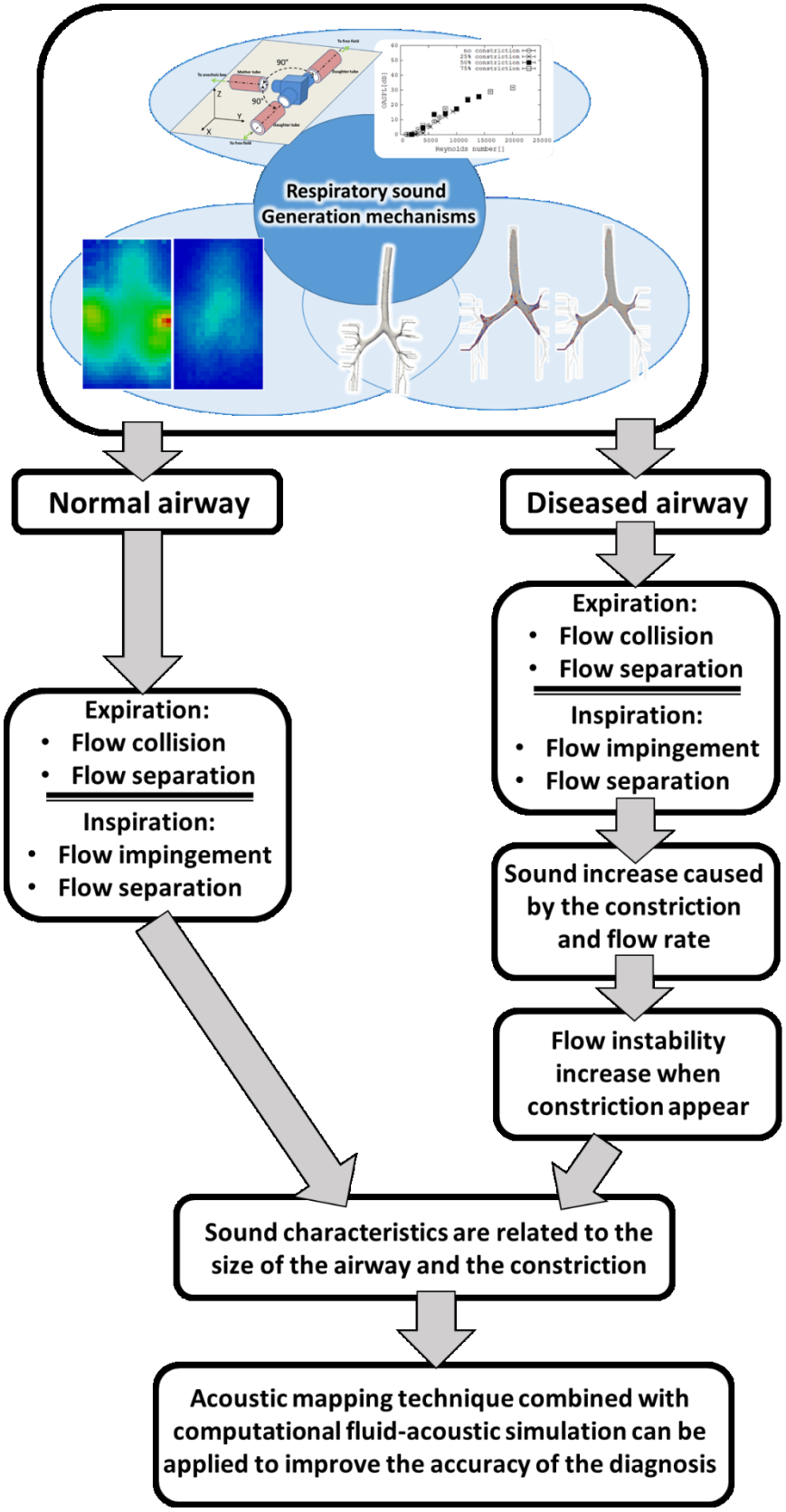

Figure 5-1. Schematic diagram of the possible sound generation mechanisms the normal and diseased airway.

Appendix A

Additional measurement using different branching configuration

Another experiment using different branching configuration was performed in order to reveal the effect of the branch geometry on the Reynolds-OASPL relationship discussed in Chapter 2. The geometry is shown in Figure A-2. This model was a branching geometry with 70 degrees branching angle and daughter-to-mother diameter ratio of 0.78 as proposed by Pedley [1].

Same method of acoustic measurements to the method used in Chapter 2 was performed. OASPL of the frequency ranges: 1-200 Hz, 200-400 Hz, 400-600 Hz, 600-800 Hz, 800-1000 Hz, and 150-10000 Hz were calculated and shown in Figure A-2.

Similar tendency was found for the generated sound in all frequency ranges. This results may indicate that the alteration of the flow disturbance at the constriction region is more dominant compared to those generated by the branching geometry. It also indicates that the sound generation is not mainly attributed to the flow behavior in the junction in the inspiration direction.

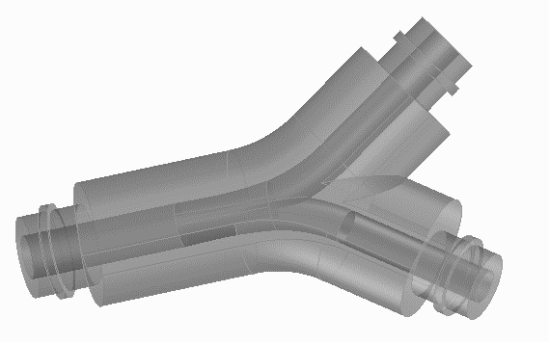

Figure A-1. Branching geometry with 70 degrees branching angle as proposed by Pedley [1].

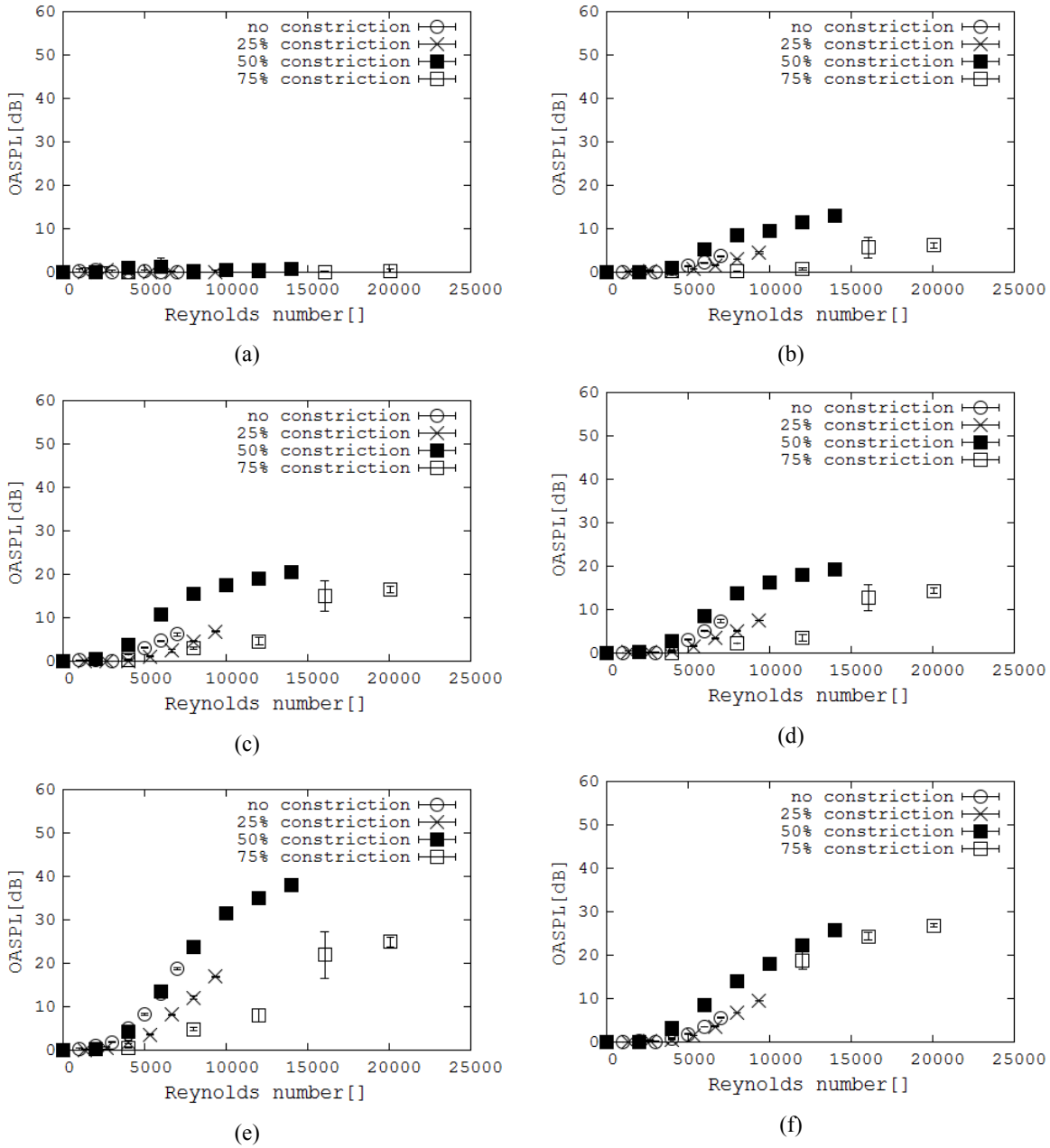

Figure A-2. OASPL of the sound measured from the model model proposed by Pedley [1]. (a) 1–200 Hz, (b) 200–400 Hz, (c) 400–600 Hz, (d) 600–800 Hz, (e) 800–1000 Hz, (f) 150–10000 Hz.

Appendix B

Tracheobronchial model geometry detail and material specification

The geometry used in this thesis was obtained from CT-scan image of an 11-years old boy. The images were taken in Minami-Wakayama Medical Center. In using the geometry model for the numerical simulations, each of the bronchi ends is named separately as shown in Figure A-1. In the experiments, the trachea is connected to 16 mm inner diameter hose, and the 39 bronchus are connected to 8 silicone tubes diameter of 2 mm, and 31 silicone tubes diameter of 1 mm.

Figure A-2 shows the branching pattern of the tracheobronchial model. According to Horsfield rule [70], this model contains the 10 generation branching configuration.

The properties of silicone material, according to the specification given by R-Tech Corp, used in this thesis are as follows,

- density at 23 °C: 1030 $kg.m^3$
- tensile strength: 4.3 MPa
- elongation at break: 350%
- tear strength (resistance): 12 $kN.m^{-1}$.

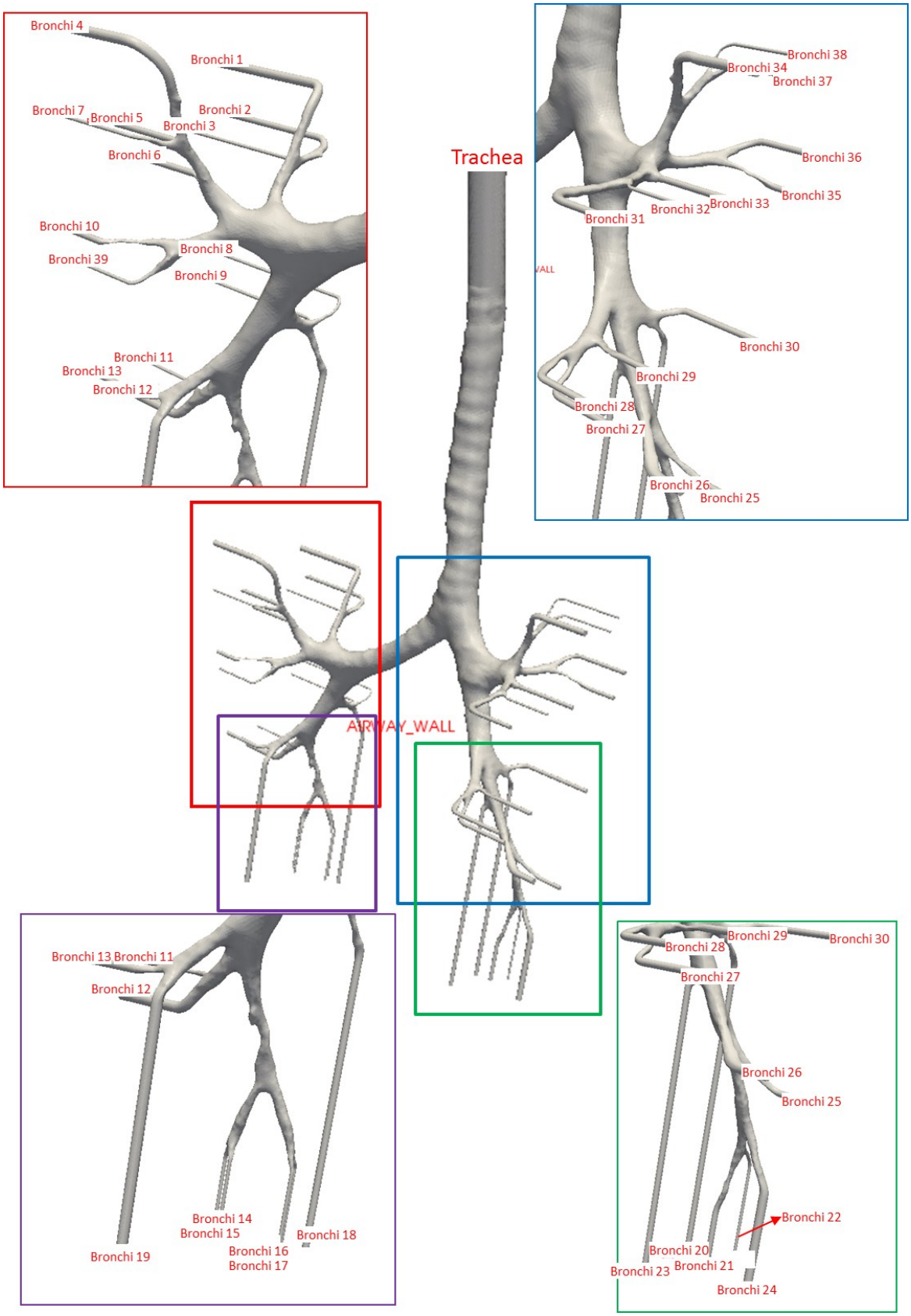

Figure B-1. Naming of the bronchi ends used for the numerical simulations.

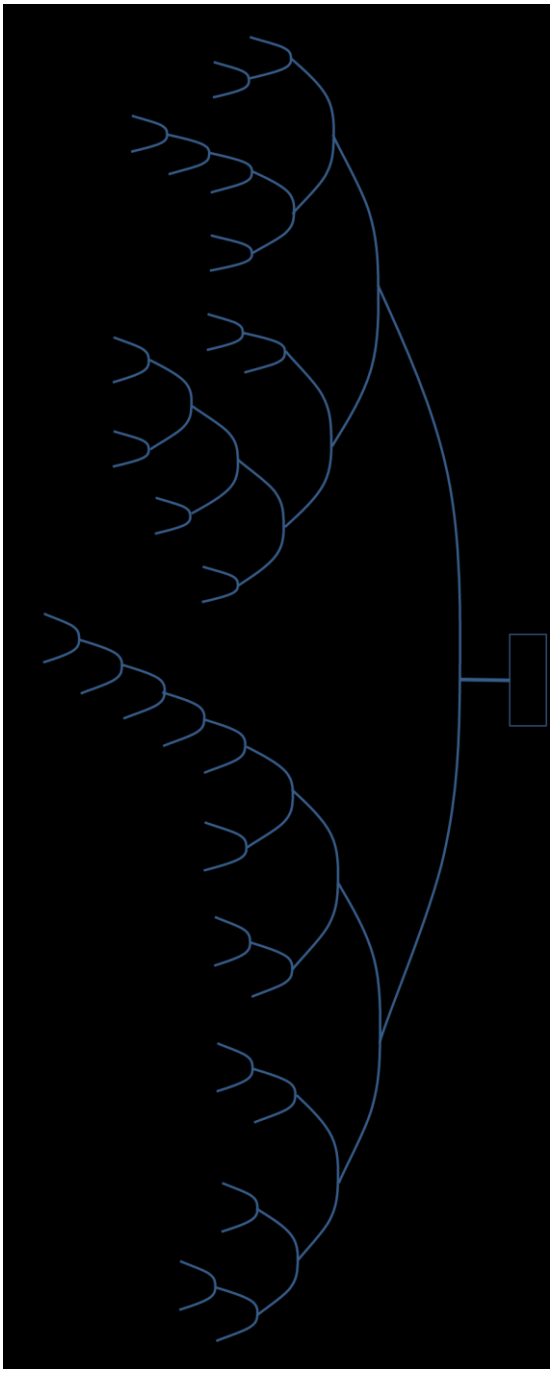

Figure B-2. Schematic diagram of the branching pattern of the silicone model used in this thesis. “b” indicates the bronchi index based on Figure A-1.

REFERENCES

[1] T. J. Pedley, "Pulmonary Fluid Dynamics," *Annu. Rev. Fluid Mech.*, vol. 9, no. 1, pp. 229–274, 1977.

[2] Z. Dai, Y. Peng, B. M. Henry, H. A. Mansy, R. H. Sandler, and T. J. Royston, "A comprehensive computational model of sound transmission through the porcine lung," *J. Acoust. Soc. Am.*, vol. 136, no. 3, pp. 1419–1429, Sep. 2014.

[3] Z. Dai, Y. Peng, H. A. Mansy, R. H. Sandler, and T. J. Royston, "Experimental and computational studies of sound transmission in a branching airway network embedded in a compliant viscoelastic medium," *J. Sound Vib.*, vol. 339, pp. 215–229, 2015.

[4] L. P. Malmberg, R. Sorva, and A. R. A. Sovijarvi, "Frequency Distribution of Breath Sounds as an Indicator of Bronchoconstriction During Histamine Challenge Test in Asthmatic Children," vol. 177, no. 1 994, pp. 170–177, 1994.

[5] K. K. Guntupalli, R. M. Reddy, R. H. Loutfi, P. M. Alapat, V. D. Bandi, and N. A. Hanania, "Evaluation of obstructive lung disease with vibration response imaging.," *J. Asthma*, vol. 45, no. 10, pp. 923–30, 2008.

[6] A. Bohadana, G. Izbicki, and S. S. Kraman, "Fundamentals of lung auscultation.," *N. Engl. J. Med.*, vol. 370, no. 8, pp. 744–51, 2014.

[7] R. L. Murphy, "Auscultation of the lung: past lessons, future possibilities.," *Thorax*, vol. 36, no. 2, pp. 99–107, 1981.

[8] F. Martini, M. J. Timmons, and R. B. Tallitsch, *Human anatomy*. Pearson Education

Limited, 2014.

[9] M. J. Lighthill, “On Sound Generated Aerodynamically. I. General Theory,” *Proc. R. Soc. A Math. Phys. Eng. Sci.*, vol. 211, no. 1107, pp. 564–587, Mar. 1952.

[10] M. J. Lighthill, “On Sound Generated Aerodynamically. II. Turbulence as a Source of Sound,” *Proc. R. Soc. A Math. Phys. Eng. Sci.*, vol. 222, no. 1148, pp. 1–32, 1954.

[11] J. F. Bullar, “Experiments to Determine the Origin of the Respiratory Sounds,” *Proc. R. Soc. London*, vol. 37, no. 232–234, pp. 411–422, 1884.

[12] F. Dalmay, M. T. Antonini, P. Marquet, and R. Menier, “Acoustic properties of the normal chest,” *Eur. Respir. J.*, vol. 8, no. 10, pp. 1761–1769, 1995.

[13] R. Loudon and R. L. Murphy, “Lung sounds.,” *Am. Rev. Respir. Dis.*, vol. 130, no. 4, pp. 663–673, 1984.

[14] P. Forgacs, “Lung Sounds,” *Britanical J. Dis. Chest*, vol. 63, pp. pp.1–12, 1969.

[15] P. Forgacs, A. R. Nathoo, and H. D. Richardson, “Breath sounds.,” *Thorax*, vol. 26, no. 3, pp. 288–95, May 1971.

[16] M. Munakata, Y. Homma, M. Matsuzaki, H. Ogasawara, K. Tanimura, H. Kusaka, and Y. Kawakami, “Production mechanism of crackles in excised normal canine lungs.,” *J. Appl. Physiol.*, vol. 61, no. 3, pp. 1120–1125, 1986.

[17] A. Vyshedskiy, R. M. Alhashem, R. Paciej, and M. Ebril, “Mechanism of Inspiratory and Expiratory Crackles *,” 2015.

[18] A. B. Almeida, S. V. Buldyrev, and A. M. Alencar, “Crackling sound generation during the formation of liquid bridges: A lattice gas model,” *Phys. A Stat. Mech. its Appl.*, vol. 392, no. 16, pp. 3409–3416, 2013.

[19] S. Charleston-villalobos, G. Dorantes-me, and G. Chi-lem, “Acoustic thoracic image of crackle sounds using linear and nonlinear processing techniques,” pp. 15–24, 2011.

[20] J. B. Grotberg, “Flutter in flow-limited collapsible tubes : a mechanism for generation of wheezes,” no. 5, 1989.

[21] M. Weinberger and M. Abu-Hasan, “Pseudo-asthma: when cough, wheezing, and dyspnea are not asthma.,” *Pediatrics*, vol. 120, no. 4, pp. 855–864, 2007.

[22] N. Gavriely, Y. Palti, G. Alroy, and J. B. Grotberg, “Measurement and theory of wheezing breath sounds.,” *J. Appl. Physiol.*, vol. 57, no. 2, pp. 481–492, 1984.

[23] R. P. Baughman and R. G. Loudon, “Lung sound analysis for continuous evaluation of airflow obstruction in asthma,” *Chest*, vol. 88, no. 3, pp. 364–368, 1985.

[24] K. Bauer, H. Chaves, and C. Brücker, “Visualizing flow partitioning in a model of the upper human lung airways.,” *J. Biomech. Eng.*, vol. 132, no. 3, p. 031005, 2010.

[25] T. J. Pedley, R. C. Schroter, and M. F. Sudlow, “The prediction of pressure drop and variation of resistance within the human bronchial airways,” *Respir. Physiol.*, vol. 9, no. 3, pp. 387–405, 1970.

[26] M. Brouns, S. T. Jayaraju, C. Lacor, J. De Mey, M. Noppen, W. Vincken, and S. Verbanck, “Tracheal stenosis : a flow dynamics study,” *J. Appl. Physiol.*, vol. 102, pp. 1178–1184,

2007.

[27] S. T. Jayaraju, M. Brouns, C. Lacor, B. Belkassem, and S. Verbanck, “Large eddy and detached eddy simulations of fluid flow and particle deposition in a human mouth-throat,” *J. Aerosol Sci.*, vol. 39, no. 10, pp. 862–875, 2008.

[28] C. L. Lin, M. H. Tawhai, G. McLennan, and E. A. Hoffman, “Characteristics of the turbulent laryngeal jet and its effect on airflow in the human intra-thoracic airways,” *Respir. Physiol. Neurobiol.*, vol. 157, no. 2–3, pp. 295–309, 2007.

[29] M. H. Tawhai and C. L. Lin, “Airway gas flow,” *Compr. Physiol.*, vol. 1, no. 3, pp. 1135–1157, 2011.

[30] E. M. Saber and G. Heydari, “Flow patterns and deposition fraction of particles in the range of 0.1-10μm at trachea and the first third generations under different breathing conditions,” *Comput. Biol. Med.*, vol. 42, no. 5, pp. 631–638, 2012.

[31] Z. Zhang and C. Kleinstreuer, “Airflow structures and nano-particle deposition in a human upper airway model,” *J. Comput. Phys.*, vol. 198, pp. 178–210, 2004.

[32] R. B. Schlesinger and D. E. Bohning, “PARTICLE DEPOSITION IN A HOLLOW CAST OF THE The respiratory tract is the main portal of entry for airborne particulates , many of which are capable of producing injury , or disease . The pattern of particle deposition is a major determinant of pathogenic ,” *Environ. Heal.*, vol. 8, 1977.

[33] J. K. Comer, C. Kleinstreuer, and C. S. Kim, “Flow structures and particle deposition patterns in double-bifurcation airway models. Part 2. Aerosol transport and deposition,” vol. 435, pp. 55–80, 2001.

[34] Y. Zhang and W. Finlay, “Measurement of the Effect of Cartilaginous Rings on Particle Deposition in a Proximal Lung Bifurcation Model,” *Aerosol Sci. Technol.*, vol. 39, no. June 2012, pp. 394–399, 2005.

[35] D. K. Walters and W. H. Luke, “Computational fluid dynamics simulations of particle deposition in large-scale, multigenerational lung models.,” *J. Biomech. Eng.*, vol. 133, no. 1, p. 011003, 2011.

[36] Z. Li, C. Kleinstreuer, and Z. Zhang, “Particle deposition in the human tracheobronchial airways due to transient inspiratory flow patterns,” *J. Aerosol Sci.*, vol. 38, no. 6, pp. 625–644, 2007.

[37] R. Beck, G. Rosenhouse, M. Mahagnah, R. M. Chow, D. W. Cugell, and N. Gavriely, “Measurements and theory of normal tracheal breath sounds,” *Ann. Biomed. Eng.*, vol. 33, no. 10, pp. 1344–1351, 2005.

[38] A. B. Bohadana, R. Peslin, and H. Uffholtz, “Breath sounds in the clinical assessment of airflow obstruction.,” *Thorax*, vol. 33, no. 3, pp. 345–51, 1978.

[39] J. B. Grotberg and S. H. Davis, “Fluid-dynamic flapping of a collapsible channel: sound generation and flow limitation.,” *J. Biomech.*, vol. 13, no. 3, pp. 219–230, 1980.

[40] W. C. P. van der Velden, A. H. van Zuijlen, A. T. de Jong, C. T. Lynch, L. J. Hoeve, and H. Bijl, “Acoustic simulation of a patient’s obstructed airway,” *Comput. Methods Biomech. Biomed. Engin.*, vol. 19, no. 2, pp. 144–158, Jan. 2016.

[41] Z. Zhang, L. Mongeau, S. H. Frankel, S. Thomson, and J. B. Park, “Sound generation by steady flow through glottis-shaped orifices.,” *J. Acoust. Soc. Am.*, vol. 116, no. 3, pp.

1720–1728, 2004.

[42] J. Earis, “Lung sounds.,” *Thorax*, vol. 47, no. 9, pp. 671–672, 1992.

[43] J. C. Hardin and J. L. Patterson, “Monitoring the state of the human airways by analysis of respiratory sound,” *Acta Astronaut.*, vol. 6, no. 9, pp. 1137–1151, 1979.

[44] S. S. Kraman and P. M. Wang, “Air-flow generated sound in a hollow canine airway cast,” *Chest*, vol. 97, no. 2, pp. 461–466, 1990.

[45] O. Austrheim and S. S. Kraman, “The effect of low density gas breathing on vesicular lung sounds,” *Respir. Physiol.*, vol. 60, no. 2, pp. 145–155, 1985.

[46] M. Mahagnah and N. Gavriely, “Gas density does not affect pulmonary acoustic transmission in normal men.,” *J. Appl. Physiol.*, vol. 78, no. 3, pp. 928–37, 1995.

[47] N. Meslier, G. Charbonneau, and J.-L. Racineux, “Wheezes,” *Eur. Respir. J.*, vol. 8, no. 11, pp. 1942–1948, 1995.

[48] C. Habukawa, K. Murakami, N. Horii, M. Yamada, and Y. Nagasaka, “A new modality using breath sound analysis to evaluate the control level of asthma.,” *Allergol. Int.*, vol. 62, no. 1, pp. 29–35, 2013.

[49] C. Habukawa, Y. Nagasaka, K. Murakami, and T. Takemura, “High-pitched breath sounds indicate airflow limitation in asymptomatic asthmatic children,” *Respirology*, vol. 14, no. 3, pp. 399–403, 2009.

[50] L. P. Malmberg, L. Pesu, and A. R. A. Sovijarvi, “Significant differences in flow

standardised breath sound spectra in patients with chronic obstructive pulmonary disease , stable asthma , and healthy lungs," pp. 1285–1291, 1995.

[51] H. Yokoyama, A. Miki, H. Onitsuka, and A. Iida, "Direct numerical simulation of fluid–acoustic interactions in a recorder with tone holes," *J. Acoust. Soc. Am.*, vol. 138, no. 2, pp. 858–873, 2015.

[52] D. J. McKinzie Jr. and R. J. Burns, "Analysis of noise produced by jet impingement near the trailing edge of a flat and a curved plate," vol. 7, no. January, 1975.

[53] M. J. Fisher, P. A. Lush, and M. Harper Bourne, "Jet noise," *J. Sound Vib.*, vol. 28, no. 3, pp. 563–585, Jun. 1973.

[54] M. L. Shur, P. R. Spalart, M. K. Strelets, and a. K. Travin, "Towards the prediction of noise from jet engines," *Int. J. Heat Fluid Flow*, vol. 24, no. 4, pp. 551–561, 2003.

[55] M. Ikeda and T. Mitsumoji, "Evaluation Method of Low-Frequency Aeroacoustic Noise Source Structure Generated by Shinkansen Pantograph," *Q. Rep. RTRI*, vol. 49, no. 3, pp. 184–190, 2008.

[56] M. K. Bull and M. P. Norton, "On the hydrodynamic and acoustic wall pressure fluctuations in turbulent pipe flow due to a 90?? mitred bend," *J. Sound Vib.*, vol. 76, no. 4, pp. 561–586, 1981.

[57] S. Dequand, S. J. Hulshoff, Y. Auregan, J. Hujnen, R. ter Riet, L. J. van Lier, and A. Hirschberg, "Acoustic of 90 degree sharp bends. Part II: Low-frequency aeroacoustical response," *Acta Acust. united with Acust.*, vol. 90, no. M, pp. 13–23, 2004.

[58] R. Hiramoto and H. Higuchi, “Vortex shedding behind a nonparallel pair of circular cylinders,” *J. Fluids Struct.*, vol. 18, no. 1, pp. 131–143, 2003.

[59] O. Inoue, W. Iwakami, and N. Hatakeyama, “Aeolian tones radiated from flow past two square cylinders in a side-by-side arrangement,” *Phys. Fluids*, vol. 18, no. 4, 2006.

[60] T. Kambe, “Vortex Sound: CFD and Experimental Observation,” *Accc.Riken.Jp*, pp. 23–24, 2009.

[61] M. Piellard, “Application to the case of a ducted diaphragm at low Mach number,” in *AIAA Aeroacoustics Conference*, 2008, no. May, p. 2873.

[62] H. Yokoyama and A. Iida, “Aerodynamic Sound Sources from Flows around a Rectangular Cylinder with a Low Mach Number,” *Trans. JAPAN Soc. Mech. Eng. Ser. B*, vol. 79, no. 799, pp. 344–355, 2013.

[63] H. Y. Luo and Y. Liu, “Modeling the bifurcating flow in a CT-scanned human lung airway,” *J. Biomech.*, vol. 41, no. 12, pp. 2681–2688, 2008.

[64] J. Choi, M. H. Tawhai, E. A. Hoffman, and C. L. Lin, “On intra- and intersubject variabilities of airflow in the human lungs,” *Phys. Fluids*, vol. 21, no. 10, pp. 1–17, 2009.

[65] E. R. Weibel, *Morphometry of the Human Lung*. Berlin, Heidelberg: Springer Berlin Heidelberg, 1963.

[66] R. C. Schroter and M. F. Sudlow, “Flow patterns in models of the human bronchial airways,” *Respir. Physiol.*, vol. 7, no. 3, pp. 341–355, 1969.

[67] C. H. Zhang, Y. Liu, R. M. C. So, and N. Phan-Thien, “The influence of inlet velocity profile on three-dimensional three-generation bifurcating flows,” *Comput. Mech.*, vol. 29, no. 4–5, pp. 422–429, 2002.

[68] K. Horsfield and G. Cumming, “Angles of branching and diameters of branches in the human bronchial tree,” *Bull. Math. Biophys.*, vol. 29, no. 2, pp. 245–259, 1967.

[69] K. Horsfield and G. Cumming, “Morphology of the bronchial tree in man,” *J. Appl. Physiol.*, vol. 24, no. 3, pp. 373–83, Mar. 1968.

[70] K. Horsfield, G. Dart, and D. Olson, “Models of the human bronchial tree,” *J. Appl. Physiol.*, vol. 31, no. 2, pp. 207–217, 1971.

[71] V. P. Harper, H. Pasterkamp, H. Kiyokawa, and G. R. Wodicka, “Modeling and measurement of flow effects on tracheal sounds,” *IEEE Trans. Biomed. Eng.*, vol. 50, no. 1, pp. 1–10, 2003.

[72] A. Y. M. Jones, R. D. Jones, K. Kwong, and Y. Burns, “The effect on sound generation of varying both gas flow rate and the viscosity of sputum-like gel in a simple tubular model,” *Lung*, vol. 178, no. 1, pp. 31–40, 2000.

[73] H. J. Schreur, P. J. Sterk, J. Vanderschoot, H. C. van Klink, E. van Vollenhoven, and J. H. Dijkman, “Lung sound intensity in patients with emphysema and in normal subjects at standardised airflows.,” *Thorax*, vol. 47, no. 9, pp. 674–679, 1992.

[74] T. Sera, S. Satoh, H. Horinouchi, K. Kobayashi, and K. Tanishita, “Respiratory Flow in a Realistic Tracheostenosis Model,” *J. Biomech. Eng.*, vol. 125, no. August, pp. 461–471, 2003.

[75] Y. Liu, R. M. C. So, and C. H. Zhang, “Modeling the bifurcating flow in a human lung airway,” vol. m, pp. 465–473, 2002.

[76] S. Zarei, A. Mirtar, B. Andresen, and P. Salamon, “Modeling the airflow in a lung with cystic fibrosis,” vol. i, pp. 119–140, 2013.

[77] R. S. McNeill, G. D. Malcolm, and W. R. Brown, “A Comparison of Expiratory and Inspiratory Flow Rates in Health and in Chronic Pulmonary Disease,” *Thorax*, vol. 14, pp. 225–231, 1959.

[78] H. J. W. Schreur, J. Vanderschoot, a. H. Zwinderman, J. H. Dijkman, and P. J. Sterk, “The effect of methacholine-induced acute airway narrowing on lung sounds in normal and asthmatic subjects,” *Eur. Respir. J.*, vol. 8, no. 2, pp. 257–265, 1995.

[79] M. H. Krane, “Aeroacoustic production of low-frequency unvoiced speech sounds,” *J. Acoust. Soc. Am.*, vol. 118, no. 1, p. 410, 2005.

[80] D. P. S. Spence, S. Bentley, D. H. Evans, M. D. L. Morgan, and S. Bentley, “Effect of methacholine induced bronchoconstriction on the spectral characteristics of breath sounds in asthma,” pp. 680–683, 2000.

[81] S. Bell, S. Member, N. West, and I. T. Heory, “Acoustic Beamforming : System Theory and Requirements,” *Source*, no. 2.

[82] J. Hald, “Combined NAH and Beamforming Using the Same Microphone Array,” *Sound Vib.*, no. December, pp. 18–25, 2004.

[83] F. Deblauwe, K. Jansen, and M. Robin, “Extending the usability of near-field acoustic

holography and beamforming by using focalization," *14th Int. Congr. Sound Vib.*, pp. 1–8, 2007.

[84] B. Rafaely, "Analysis and design of spherical microphone arrays," *IEEE Trans. Speech Audio Process.*, vol. 13, no. 1, pp. 135–143, 2005.

[85] R. P. Dellinger, J. E. Parrillo, A. Kushnir, M. Rossi, and I. Kushnir, "Dynamic visualization of lung sounds with a vibration response device: A case series," *Respiration*, vol. 75, no. 1, pp. 60–72, 2008.

[86] M. Yosef, R. Langer, S. Lev, and Y. A. Glickman, "Effect of airflow rate on vibration response imaging in normal lungs," *Open Respir. Med. J.*, vol. 3, pp. 116–122, 2009.

[87] J. Meyer, P. J. Friedman, T. M. Maher, and J. M. Madison, "Vibration Response Imaging Technology in Healthy Subjects," no. September, pp. 845–852, 2008.

[88] A. C. Mehta, M. Gat, S. Mann, and J. M. Madison, "Accuracy of gray-scale coding in lung sound mapping," *Comput. Med. Imaging Graph.*, vol. 34, no. 5, pp. 362–369, 2010.

[89] M. Nakamura, S. Wada, T. Miki, Y. Shimada, Y. Suda, and G. Tamura, "Automated segmentation and morphometric analysis of the human airway tree from multidetector CT images.," *J. Physiol. Sci.*, vol. 58, no. 7, pp. 493–498, 2008.

[90] V. Gross, A. Dittmar, T. Penzel, F. Schüttler, and P. Von Wichert, "The relationship between normal lung sounds, age, and gender," *Am. J. Respir. Crit. Care Med.*, vol. 162, no. 3 I, pp. 905–909, 2000.

[91] H. Pasterkamp and S. Patel, "Asymmetry of respiratory sounds and thoracic transmission,"

Med. Biol. Eng. Comput., vol. 35, pp. 103–106, 1997.

[92] T. Gemci, V. Ponyavin, Y. Chen, H. Chen, and R. Collins, "CFD Simulation of Airflow in a 17-Generation Digital reference model of the human bronchial tree," *J Biomech*, vol. 23, no. 1, pp. 5–18, 2007.

[93] T. B. Martonen, L. Quan, Z. Zhang, and C. J. Musante, "Flow simulation in the human upper respiratory tract.," *Cell Biochem. Biophys.*, vol. 37, no. 1, pp. 27–36, 2002.

[94] S. Thesis and V. Deun, "Simulation of airflow in a realistic CT- scan derived lung geometry Simulation of airflow in a realistic CT- scan derived lung geometry," 2011.

[95] Y. Yin, J. Choi, E. A. Hoffman, M. H. Tawhai, and C. L. Lin, "Simulation of pulmonary air flow with a subject-specific boundary condition," *J. Biomech.*, vol. 43, no. 11, pp. 2159–2163, 2010.

[96] P. W. L. Ã and S. Vinchurkar, "Validating CFD predictions of respiratory aerosol deposition : Effects of upstream transition and turbulence," vol. 40, pp. 305–316, 2007.

[97] C. Kleinstreuer, Z. Zhang, and J. F. Donohue, "Targeted Drug-Aerosol Delivery in the Human Respiratory System," 2008.

[98] D. K. Lilly, "A Proposed Modification of the Germano-Subgrid-Scale Closure Method," *Phys. Fluids a-Fluid Dyn.*, vol. 4, no. 3, pp. 633–635, 1992.

[99] M. S. Mathias, E. M. Gennaro, and M. A. F. Medeiros, "Vortex Generation and Aeroacoustics in Asymmetric Wakes," *Procedia IUTAM*, vol. 14, pp. 590–594, 2015.

[100] M. S. Howe, *Theory of Vortex Sound*. Cambridge: Cambridge University Press, 2002.

PUBLICATION LIST

ORIGINAL PAPERS

1) Gabriel Pramudita Saputra, Kazunori Nozaki, Satoshi Ii, Shigeo Wada, "Aeroacoustic sound alteration in airway bronchoconstriction represented by a constricted T-branch model", Journal of Biomechanical Science and Engineering, Vol. 10, No. 1 (2014).

INTERNATIONAL CONFERENCES

1) Gabriel Pramudita Saputra, Kazunori Nozaki, Satoshi Ii, Chizu Habukawa, Shigeo Wada, "Acoustic visualisation of flow-sound in the respiratory airway," Summer Biomechanics, Bioengineering and Biotransport Conference, 2 pages, Maryland, USA (June 2016).

2) Gabriel Pramudita Saputra, Kazunori Nozaki, Satoshi Ii, Chizu Habukawa, Shigeo Wada, "Acoustic source detection of realistic airway model using microphone array system and aeroacoustic analysis," Eight Asian-Pacific Conference on Biomechanics, 1 page, Hokkaido, Japan (September 2015).

3) Gabriel Pramudita Saputra, Kazunori Nozaki, Satoshi Ii, Chizu Habukawa, Shigeo Wada, "Acoustic detection of respiratory sounds in silicone lung airway model using microphone array system," Summer Biomechanics, Bioengineering and Biotransport Conference, 2 pages, Salt Lake City, USA (June 2015).

4) Gabriel Pramudita Saputra, Kazunori Nozaki, Satoshi Ii, Shigeo Wada, "A preliminary experimental study on the sound generation by flow impingement in branching airway,"

The 15th International Conferences on Biomedical Engineering, 4 pages, National University of Singapore, Singapore (December 2013)

5) Gabriel Pramudita Saputra, Kazunori Nozaki, Satoshi Ii, Shigeo Wada, "Experimental flow-sound analyses in T-branch for understanding lung sound production mechanisms," Internoise 2013 the 42nd International Congress and Exposition on Noise Control Engineering, 13 pages, Innsbruck, Austria (September 2013).

DOMESTIC CONFERENCE

1) Gabriel Pramudita Saputra, Kazunori Nozaki, Satoshi Ii, Shigeo Wada, "Aeroacoustic analysis of lung sound using branching airway models," Biofrontier Symposium 2013, Kyoto (November 2013).

REVIEW

1) 和田 成生, Gabriel Pramudita Saputra, 杉谷 和哉, 伊井 仁志, 土生川 千珠, "気道における空力音の発生と伝播―流体音響工学からの呼吸音の理解―,"日本小児アレルギー学会誌, Vol. 29 No. 1 p. 58-64 (2015).

ACKNOWLEGDEMENT

I would like to acknowledge the contribution and supports from many people so that this study can be accomplished. First of all, I would like to express my gratitude to Professor Shigeo Wada for the guidance, patience, and supervision throughout this study. It is a great chance for me to study in one of the biomechanics laboratories in Japan. I am grateful to Research Associate Professor Satoshi Ii and Associate Professor Kenichiro Koshiyama for the advice, insight, and support to conduct a good research. I would like to express my huge appreciation to Professor Kazunori Nozaki for his supporting research discussion and motivation throughout my study, his joyful life is teaching me how I should conduct my research in full of happiness and enjoyment.

I sincerely thank for Professor Kazuyasu Sugiyama and Professor Masao Tanaka for their support as the thesis defense committee members. It is a great chance for me to have a discussion with the expert in their field of study and to have them in reviewing this thesis. The discussion in every defense teach me many things of the fluid dynamics field and the research life style.

I would like also to thanks Dr. Chizu Habukawa for the insightful discussion regarding the physiological knowledge of the respiratory sound and anatomical information of the respiratory diseases. Additionally, I must express a big thanks to Tomohiro Otani, Taiki Shigematsu, Narihiko Koike, Tsukasa Yoshinaga for the interesting yet insightful talks of the research and daily life, and also for all members in the Wada Laboratory for the nice environment in research. It has been a good experience to have the research in Wada Laboratory for the recent 5 years.

Nothing is more important than a family, and I would like to thanks all of my big family members wherever you are for the support before I came to Japan, when I am studying here in Japan until I finish my study. Without your help I will never be able to come here. My big

thanks also to my family in Japan, Keluarga Katolik Kansai, Persatuan Pelajar Indonesia Osaka Nara, Keluarga Toyonaka, and all Indonesian community and relatives in Japan.

I would like also to show my appreciation for the funding support of the living and studying cost from the Japan Ministry of Education, Culture, Sports, Science and Technology through the MEXT Scholarship of the 21st Century Program in Graduate School of Engineering Science.

Gabriel Pramudita Saputra

Department of Mechanical Science and Bioengineering

Graduate School of Engineering Science

Osaka University